bioRxiv preprint doi: https://doi.org/10.1101/2021.03.31.437934; this version posted March 31, 2021. The copyright holder for this preprint (which was not certified by peer review) is the author/funder, who has granted bioRxiv a license to display the preprint in perpetuity. It is made available under aCC-BY-ND 4.0 International license.

Unipolar peptidoglycan synthesis in the Rhizobiales requires an essential class A penicillin-binding protein

Michelle A. Williams[1*], Alena Aliashkevich[2], Elizaveta Krol[3], Erkin Kuru[4+], Jacob M. Bouchier[1], Jonathan Rittichier[6+], Yves V. Brun[5], Michael S. VanNieuwenhze[6], Anke Becker[3], Felipe Cava[2] and Pamela J. B. Brown[1]

[1]Division of Biological Sciences, University of Missouri, Columbia, Missouri, United States
[2]Department of Molecular Biology, Laboratory for Molecular Infection Medicine Sweden (MIMS), Centre for Microbial Research, Umeå University, Umeå, Sweden
[3]Center for Synthetic Microbiology (SYNMIKRO) and Department of Biology, PhilippsUniversität Marburg, Marburg, Germany
[4]Department of Chemistry, Indiana University, Bloomington, Indiana, United States
[5] Département de microbiologie, infectiologie et immunologie, Faculté de médecine, Université de Montréal

[*]Current address: Department of Biology, McMaster University, Hamilton, Ontario, Canada
[+]Current address: Department of Genetics, Harvard Medical School, Boston, Massachusetts, United States

bioRxiv preprint doi: https://doi.org/10.1101/2021.03.31.437934; this version posted March 31, 2021. The copyright holder for this preprint (which was not certified by peer review) is the author/funder, who has granted bioRxiv a license to display the preprint in perpetuity. It is made available under aCC-BY-ND 4.0 International license.

ABSTRACT

Members of the Rhizobiales are polarly-growing bacteria that lack homologs of the canonical rod complex. To investigate the mechanisms underlying polar cell wall synthesis, we systematically probed the function of cell wall synthesis enzymes in the plant-pathogen *Agrobacterium tumefaciens*. The development of fluorescent D-amino acid dipeptide (FDAAD) probes, which are incorporated into peptidoglycan by penicillin-binding proteins in *A. tumefaciens*, enabled us to monitor changes in growth patterns in the mutants. Use of these fluorescent cell wall probes and peptidoglycan compositional analysis convincingly demonstrate that a single class A penicillin-binding protein is essential for polar peptidoglycan synthesis. Furthermore, we find evidence of an alternative mode of cell wall synthesis that likely requires LD-transpeptidase activity. Genetic analysis and cell wall targeting antibiotics reveal that the mechanism of unipolar growth is conserved in *Sinorhizobium* and *Brucella*. This work provides insights into unipolar peptidoglycan biosynthesis employed by the Rhizobiales during cell elongation.

bioRxiv preprint doi: https://doi.org/10.1101/2021.03.31.437934; this version posted March 31, 2021. The copyright holder for this preprint (which was not certified by peer review) is the author/funder, who has granted bioRxiv a license to display the preprint in perpetuity. It is made available under aCC-BY-ND 4.0 International license.

INTRODUCTION

Our current understanding of peptidoglycan (PG) assembly in rod-shaped bacteria stems largely from investigations conducted using well-known model species like *Escherichia coli* and *Bacillus subtilis*, which incorporate new cell wall material along the lateral sidewalls of the cell body. Expanding our studies of cell wall synthesis to include diverse species, with alternative modes of elongation, is an important step in unveiling the mechanisms of how and why bacteria evolve novel growth modes and generate innovative morphologies. It had, for example, long been assumed that all rod-shaped bacteria employed the same growth strategy; however, unipolar growth is widespread among rod-shaped bacteria in the Alphaproteobacterial order Rhizobiales, suggesting diversification of growth strategies [1]. The Rhizobiales are comprised of diverse bacteria with respect to both their cellular morphology, and their environmental niches [2, 3]. This includes many species of medical and agricultural significance such as the facultative intracellular pathogens *Bartonella* and *Brucella*, the nitrogen-fixing plant symbiont *Sinorhizobium*, and the causative agent of crown gall disease *Agrobacterium tumefaciens*, [4, 5]. PG labeling experiments in *A. tumefaciens*, *Brucella abortus*, and *S. meliloti* have confirmed that unipolar growth is the mode of elongation utilized by these rod-shaped species [1]. Remarkably, labeling experiments have revealed that polar growth in *A. tumefaciens* results specifically in the incorporation of pentapeptides at the growth tip; [6] however, the mechanisms that underlie polar PG biosynthesis remain poorly understood.

bioRxiv preprint doi: https://doi.org/10.1101/2021.03.31.437934; this version posted March 31, 2021. The copyright holder for this preprint (which was not certified by peer review) is the author/funder, who has granted bioRxiv a license to display the preprint in perpetuity. It is made available under aCC-BY-ND 4.0 International license.

PG biosynthesis is an essential process that allows bacteria to grow and divide, faithfully reproducing their characteristic cell shape [7]. PG assembly requires different classes of synthesis enzymes including the penicillin-binding proteins (PBPs), which can be further divided into two classes. Class A PBPs are bifunctional enzymes that catalyze β-1,4 linkages between the N-Acetylglucosamine (NAG) and N-Acetylmuramic acid (NAM) sugars in a process called transglycosylation, and also synthesize crosslinks between 4-3 and 4-4 peptides in a process known as transpeptidation [8]. The class B PBPs are monofunctional enzymes that have only transpeptidase (TPase) activity [9]. The shape, elongation, division, sporulation (SEDS) family proteins, RodA and FtsW, also possess glycosyltransferase (GTase) activity [10, 11]. Current models of cell wall assembly maintain that SEDS proteins, in complex with their cognate class B PBP, are the primary drivers of cell wall synthesis and are required to sustain rod shape [12-14]. Thus, RodA functions with PBP2 during elongation, while FtsW functions with PBP3 (encoded by *ftsI*) during cell division. The class A PBPs are currently thought to act independently from the rod complex, functioning primarily in PG maintenance and repair [15, 16].

The suite of cell wall synthesis enzymes encoded by the Rhizobiales, is distinctly different from other bacterial orders. For example, the elongation-specific rod complex of proteins including PBP2, RodA, and MreBCD are universally absent [1, 17], suggesting that RodA-PBP2 are not the primary drivers of elongation. In addition, the genomes of Rhizobiales are enriched for the presence of LD-transpeptidases (LDTs). LDTs are a class of cell wall synthesizing enzymes that carry out transpeptidation

bioRxiv preprint doi: https://doi.org/10.1101/2021.03.31.437934; this version posted March 31, 2021. The copyright holder for this preprint (which was not certified by peer review) is the author/funder, who has granted bioRxiv a license to display the preprint in perpetuity. It is made available under aCC-BY-ND 4.0 International license.

reactions to catalyze 3-4 and 3-3 crosslinks in the cell wall [18]. The cell wall of *A. tumefaciens* contains a high proportion (30%) of 3-3 and 3-4 crosslinks, in contrast to laterally growing rod-shaped bacteria, where only 1-5% of the cell wall is crosslinked by LDTs [19]. This suggests that LDT enzymes may play an important role during polar growth [1, 20]. Overall, these observations suggest that Rhizobiales use a non-canonical mechanism for polar elongation.

Using a combination of microscopy, new probes, biochemical, and genetic analyses we have characterized the function of the six high molecular weight PBPs encoded by *A. tumefaciens* and have identified the major cell wall synthesis enzymes required for polar growth. We show that, unlike the proposed auxiliary function of PBP1a in other rod-shaped bacteria, in *A. tumefaciens* PBP1a is an essential enzyme required for polar PG expansion, with depletion of PBP1a resulting in a loss of proper rod-shape. Using newly developed fluorescent D-amino acid dipeptide (FDAAD) probes, we show that PBP1a is the enzyme primarily responsible for inserting nascent PG at the pole. Additionally, PBP1a depletion leads to a modified PG composition, including an increase in LDT linkages. Collectively, this suggests that the mechanism of polar growth in the Rhizobiales has evolved through the expansion, diversification, and altered regulation of the core cell wall synthesis machinery. We confirmed the essentiality of PBP1a in the closely related bacterium *Sinorhizobium*, suggesting that the mechanisms underlying polar growth in the Rhizobiales are well conserved. Finally, we have identified the β-lactam faropenem as a specific inhibitor of polar growth in *Agrobacterium*, *Sinorhizobium,* and *Brucella*, indicating that the target(s) of faropenem are conserved

bioRxiv preprint doi: https://doi.org/10.1101/2021.03.31.437934; this version posted March 31, 2021. The copyright holder for this preprint (which was not certified by peer review) is the author/funder, who has granted bioRxiv a license to display the preprint in perpetuity. It is made available under aCC-BY-ND 4.0 International license.

among the Rhizobiales. These findings broaden our understanding of the role of PG synthesis enzymes that contribute to polar growth and will inform strategies aimed at developing novel therapeutics that target the cell wall of polar-growing bacteria in the Rhizobiales [21, 22].

RESULTS

The class A cell wall synthase PBP1a is essential for polar growth

To begin probing the molecular determinant(s) of polar growth in *A. tumefaciens*, we sought to generate deletions of the predicted PG synthase enzymes. Although *A. tumefaciens* lacks homologs to the predicted cell elongation synthases RodA and PBP2, the genome encodes four bifunctional class A PBPs (PBP1a, PBP1b1, PBP1b2 and PBP1c), two monofunctional class B PBPs (PBP3a and PBP3b), and one monofunctional GTase, MtgA (Figures 1A, 2A). To determine which of these enzyme(s) provide the primary GTase activity in the absence of a RodA homolog, we made in-frame deletions of those genes encoding predicted GTase enzymes to further explore their contribution during cell growth or division.

Consistent with a previous transposon screen [26] it was not possible to obtain a PBP1a deletion. We therefore constructed a PBP1a depletion strain by introducing a copy of the PBP1a-encoding gene, under an IPTG-inducible promoter, at a heterologous site on the chromosome and subsequently succeeded in creating an in-frame deletion of the native gene encoding PBP1a in the presence of the IPTG inducer [27]. The PBP1a

bioRxiv preprint doi: https://doi.org/10.1101/2021.03.31.437934; this version posted March 31, 2021. The copyright holder for this preprint (which was not certified by peer review) is the author/funder, who has granted bioRxiv a license to display the preprint in perpetuity. It is made available under aCC-BY-ND 4.0 International license.

123 depletion strain grown in the presence of IPTG is referred to as + PBP1a and the
124 depletion strain grown in the absence of IPTG is referred to as - PBP1a. We confirmed
125 depletion of PBP1a in the absence of IPTG using Bocillin-FL, a fluorescent penicillin
126 derivative. Two bands were observed that could correspond to the predicted molecular
127 weight of PBP1a (~88 kDa), but only the second band was absent in PBP1a-depleted
128 cells and likely represents PBP1a protein (Supplementary Figure 1A). Strikingly, cells
129 depleted of PBP1a for 16 hours lost their rod shape, becoming shorter (Figure 1A, B)
130 and wider (Supplementary Figure 1B) and had a severe viability defect, as measured by
131 spotting serial dilutions, compared to the same strain when PBP1a is induced
132 (Supplementary Figure 1C). The addition of IPTG to wild-type *A. tumefaciens* led to a
133 slight increase in the median cell length (Figure 1B, 1C) compared to wildtype alone but
134 had no effect on cell viability or rod shape (Supplementary Figure 1B, 1C).

135

136 Of the remaining bifunctional PBPs, single deletions of the genes encoding PBP1b1,
137 PBP1b2, and PBP1c had no effect on cell length (Figure 1B, C) or cell viability
138 (Supplementary Figure 1D). Similarly, a double mutant of PBP1b1 and PBP1b2 or a
139 triple mutant of PBP1b1, PBP1b2 and PBP1c (referred to as Δ3pbp) had no obvious
140 mutant phenotype with respect to cell length (Figure 1B, C) or cell viability
141 (Supplementary Figure 1D). Thus, despite all of the predicted bifunctional PBPs being
142 produced during exponential growth of *A. tumefaciens* (Supplementary Figure 1E), our
143 data indicate that only PBP1a makes a major contribution to cell growth under standard
144 laboratory conditions. Similarly, deletion of the monofunctional GTase encoding *mtgA*
145 produced cells of normal length (Figure 1B, C). The lack of a readily observed

bioRxiv preprint doi: https://doi.org/10.1101/2021.03.31.437934; this version posted March 31, 2021. The copyright holder for this preprint (which was not certified by peer review) is the author/funder, who has granted bioRxiv a license to display the preprint in perpetuity. It is made available under aCC-BY-ND 4.0 International license.

146 phenotype in the Δ*mtgA* strain is consistent with findings in *E. coli* and *Hyphomonas*
147 *neptunium* [28-30]. Together, these data suggest that the bifunctional enzyme PBP1a,
148 which likely has both GTase and TPase activities, fulfils the role of RodA and PBP2, as
149 the primary PG synthase required for polar elongation in *A. tumefaciens*.

150

bioRxiv preprint doi: https://doi.org/10.1101/2021.03.31.437934; this version posted March 31, 2021. The copyright holder for this preprint (which was not certified by peer review) is the author/funder, who has granted bioRxiv a license to display the preprint in perpetuity. It is made available under aCC-BY-ND 4.0 International license.

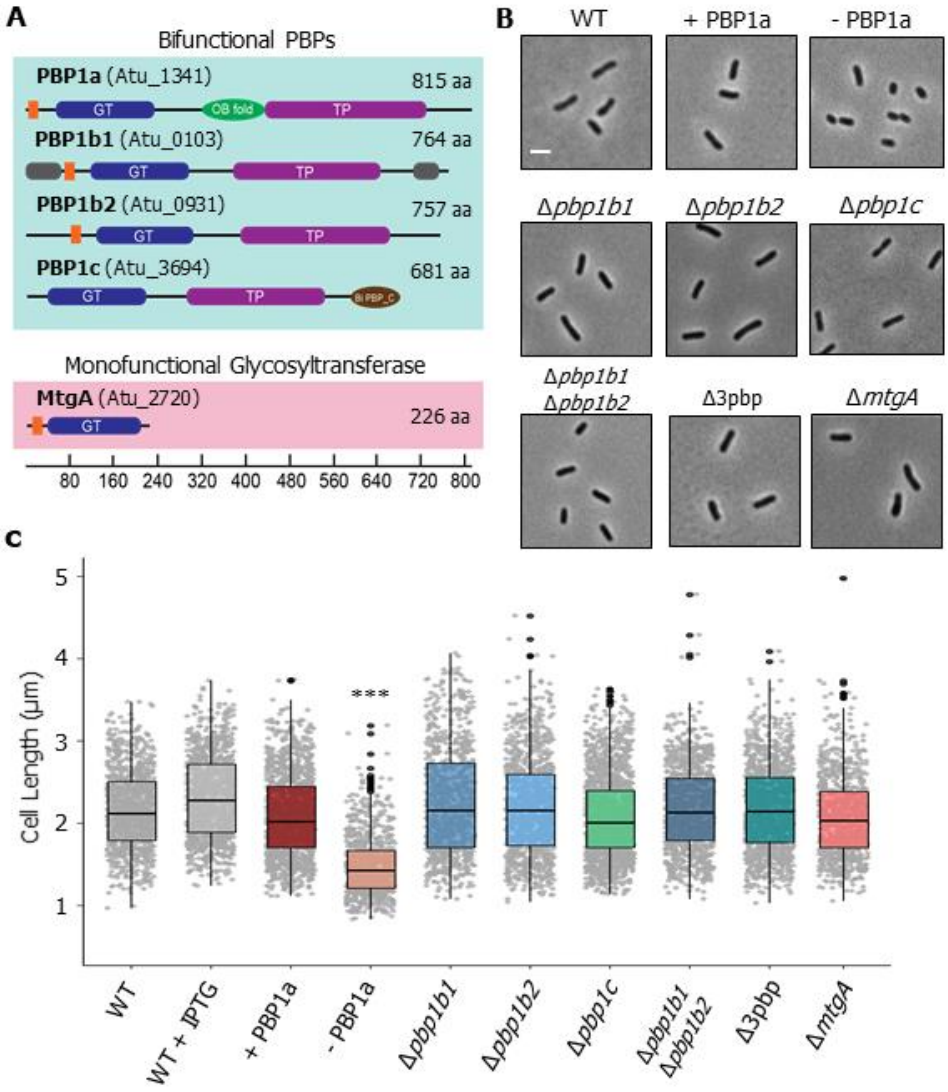

Figure 1. **Functional characterization of PG synthases in *A. tumefaciens.*** (**A**) Domain structure of the putative PG biosynthesis enzymes showing the transmembrane (orange), glycosyltransferase (GT, PF00912), transpeptidase (TP, PF00905), OB-like (PF17092), and biPBP_C (PF06832) domains. The regions of intrinsic disorder (grey) as predicted by MoBiDB are also shown [23]. The scale indicates the length in amino acids (aa). The corresponding ATU numbers are listed in parentheses beside each gene name. (**B**) Phase microscopy images showing the phenotypes of PG synthase mutants. Each strain was grown to exponential phase, spotted on an ATGN agar pad (ATGN is a minimal medium with glucose and (NH4)2SO4), and imaged by phase microscopy. Scale bar: 2 μm. (**C**) Cell length distributions of PG synthase mutants. The indicated strains were grown as in B and subjected to cell lengths measurements using MicrobeJ [24]. The data are represented as box and whisker plots in the style of Tukey [25], and visualizes five summary statistics (the center line is the median, the two hinges correspond to the first and third quartiles (the 25th and 75th percentiles), the two whiskers (representing the smallest and largest values no further than 1.5 times the interquartile range), and all "outlying" points are plotted individually. The PBP1a depletion strain grown in the presence of IPTG is referred to as + PBP1a and the depletion strain grown in the absence of IPTG is referred to as - PBP1a. Distributions of cells significantly different from wildtype (WT) are indicated (***; One-Way ANOVA with Bonferroni correction, p > 2*10^16). n = > 800 cells per strain.

bioRxiv preprint doi: https://doi.org/10.1101/2021.03.31.437934; this version posted March 31, 2021. The copyright holder for this preprint (which was not certified by peer review) is the author/funder, who has granted bioRxiv a license to display the preprint in perpetuity. It is made available under aCC-BY-ND 4.0 International license.

Class B synthases PBP3a and PBP3b are required for cell division

Incorporation of PG at the septum prior to cell division typically requires synthesis enzymes that are distinct from the cell elongation machinery. Although *A. tumefaciens* lacks the cognate SEDS-PBP pair that is typically required for elongation, the SEDS protein FtsW and PBP3, which are required for cell division, are conserved. While most bacteria possess a single, essential *ftsI* gene that encodes PBP3, some Rhizobiales, including *A. tumefaciens,* encode two FtsI homologs (PBP3a and PBP3b) (Figure 2A). *pbp3a* resides in the *mra* operon of cell division and cell envelope biogenesis genes similar to most *ftsI*-encoding homologs [31], while PBP3b is encoded as a monocistronic gene elsewhere in the genome. This raises the possibility that the second monofunctional transpeptidase (PBP3b) may serve the role of a PBP2 homolog that functions in polar elongation. Thus, we sought to determine if either of the two class B PBP homologs were required for cell division or polar elongation in *A. tumefaciens*. Saturating transposon mutagenesis in LB medium indicated that PBP3a was likely essential [26]; however, it was possible to make a deletion of *pbp3a* when cells were grown in minimal medium. These observations suggest that the PBP3a-encoding gene was conditionally essential.

In minimal medium, deletion of *pbp3a* caused a severe cell viability defect (Supplementary Figure 1F). In addition, cells were longer (Figure 2B, C), and were frequently observed to adopt branching or bulging morphologies; these features are a hallmark of cell division defects in *A. tumefaciens* [32, 33]. In contrast, deleting *pbp3b* had no effect on cell viability (Supplementary Figure 1F) or cell length (Figure 2B, C).

bioRxiv preprint doi: https://doi.org/10.1101/2021.03.31.437934; this version posted March 31, 2021. The copyright holder for this preprint (which was not certified by peer review) is the author/funder, who has granted bioRxiv a license to display the preprint in perpetuity. It is made available under aCC-BY-ND 4.0 International license.

Together, these results indicate that PBP3a is the major class B PBP contributing to cell division in *A. tumefaciens*. Since the deletion of the gene encoding PBP3a did not fully inhibit cell division, we hypothesized that PBP3b may be able to partially compensate for the loss of PBP3a. To address this possibility, we first created a PBP3a depletion strain; when this strain was grown in the absence of IPTG for 24 hours, it phenocopied the cell viability and cell length defects of the *pbp3a* deletion mutant (Figure 2B, C). We then depleted PBP3a in a Δ*pbp3b* mutant background, and found that cells not only failed to divide, but also swelled at the mid-cell before lysing (Figure 2C, Supplemental movie 1), indicating that PBP3a and PBP3b both contribute to septal PG biosynthesis during cell division. The phenotype observed in the absence of both PBP3a and PBP3b was remarkably similar to the phenotype observed during depletion of FtsW in *A. tumefaciens* [32]. FtsW possesses GTase activity, and is a major synthase required for cell division [12, 34]. Consistent with current models of cell division, we hypothesize that FtsW provides the GTase activity while PBP3a and PBP3b provide the DD-transpeptidase (TPase) activity necessary for proper septal PG biosynthesis during cell division in *A. tumefaciens*. In all, our findings support a model in which PBP3a can sustain proper cell division in the absence of PBP3b, and that, while PBP3b contributes to septal PG synthesis, it cannot fully compensate for the loss of PBP3a. Thus, both class B PBPs contribute primarily to septal PG biosynthesis.

bioRxiv preprint doi: https://doi.org/10.1101/2021.03.31.437934; this version posted March 31, 2021. The copyright holder for this preprint (which was not certified by peer review) is the author/funder, who has granted bioRxiv a license to display the preprint in perpetuity. It is made available under aCC-BY-ND 4.0 International license.

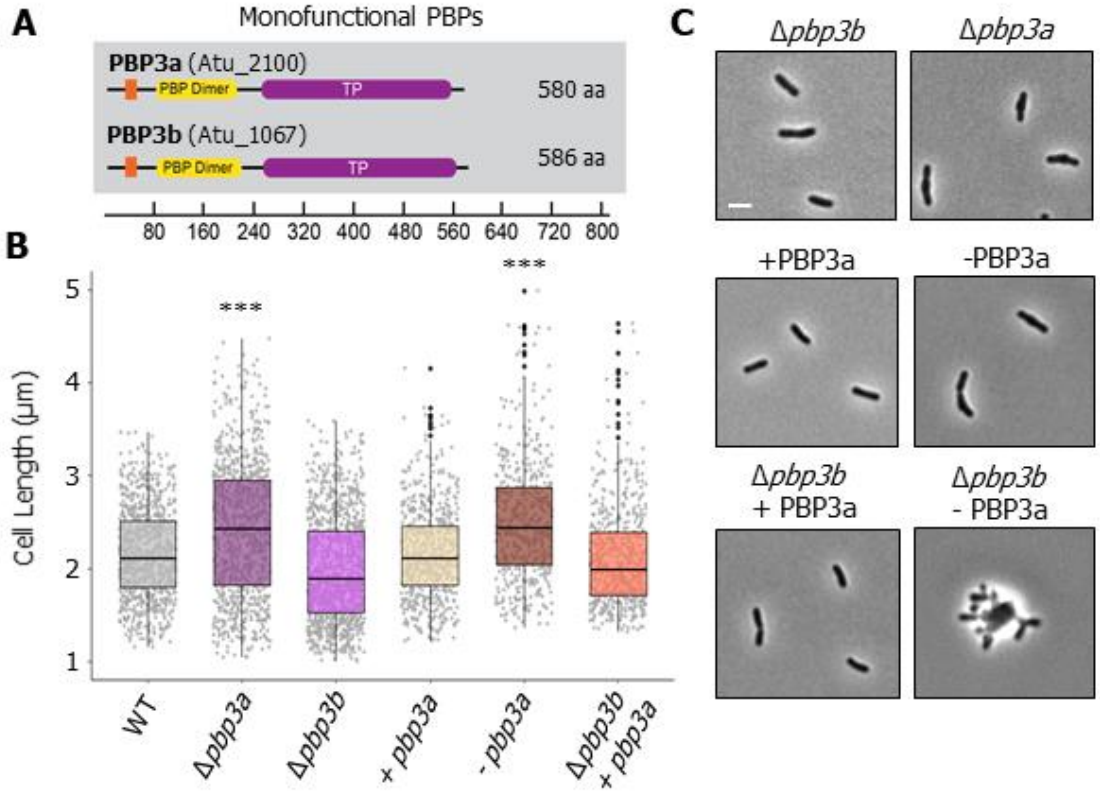

211

212 **Figure 2. Functional characterization of monofunctional synthases PBP3a and PBP3b.** (**A**) Domain
213 structure of the putative PG biosynthesis enzymes showing the transmembrane (orange), transpeptidase
214 (TP, PF00905), and PBP dimer (PF03717) domain. The scale indicates the length in amino acids (aa).
215 The corresponding ATU numbers are listed in parentheses beside each gene name. (**B**) Phase
216 microscopy images showing the phenotypes of PG synthase mutants. Each strain was grown to
217 exponential phase, spotted on an ATGN agar pad, and imaged by phase microscopy. Scale bar: 2 µm.
218 (**C**) Cell length distributions of PG synthase mutants. The indicated strains were grown to exponential
219 phase, spotted on an agar pad, imaged by phase microscopy, and subjected to cell lengths
220 measurements using MicrobeJ [24]. The data are shown as box and whisker plots in the style of Tukey
221 [25]. Distributions of cells significantly different from wildtype (WT) are indicated (***; One-Way ANOVA
222 with Bonferroni correction, p< 2*10^16). n = > 500 per strain.

223

bioRxiv preprint doi: https://doi.org/10.1101/2021.03.31.437934; this version posted March 31, 2021. The copyright holder for this preprint (which was not certified by peer review) is the author/funder, who has granted bioRxiv a license to display the preprint in perpetuity. It is made available under aCC-BY-ND 4.0 International license.

Development of new fluorescent cell wall probes to monitor PBP activity

Traditional fluorescent D-amino acid (FDAA) probes are an exceptionally useful tool for investigating the patterning of cell wall synthesis in diverse microbes [35]. However, FDAAs report on the activity of extracellular/periplasmic DD and LD transpeptidases, and as a result can be incorporated into the PG in a growth-independent mechanism [6]. Here, we have developed fluorescent D-amino acid dipeptide (FDAADs) probes to observe nascent sites of PG crosslinking in living cells, thus eliminating the need for click chemistry that is required when using traditional D-amino acid dipeptide probes (DAADs) [6, 36]. DAADs are incorporated into the cell wall precursors by the cytoplasmic MurF ligase and probe incorporation reports specifically on nascent PG synthesis [36-38]. The resulting lipid II-linked modified precursor is most likely covalently crosslinked to an existing glycan strand through the activity of bifunctional PBPs (Figure 3A). The FDAAD probe HADA—DA successfully labeled the PG of several bacteria, including *B. subtilis, E. coli, Streptomyces venezuelae and A. tumefaciens* (Figure 3B, C), and we demonstrated and evaluated PG labeling with four additional FDAADs of different sizes and molecular weights in diverse species (Supplemental figure 2A-D). In addition, *S. venezuelae,* a polar growing Actinobacteria, was short pulsed with three different FDAADs to illustrate that these probes report on the newest PG synthesis activity (Figure 3B), similar to FDAAs [39, 40]. Given their cytoplasmic mechanism of incorporation, complementary to FDAAs (which are incorporated by transpeptidases periplasmically) [6], these probes will be particularly useful to distinguish between growth-dependent and growth-independent PG crosslinking in species with a higher proportion of extracellular LDT activity, such as polar-growing bacterial species.

bioRxiv preprint doi: https://doi.org/10.1101/2021.03.31.437934; this version posted March 31, 2021. The copyright holder for this preprint (which was not certified by peer review) is the author/funder, who has granted bioRxiv a license to display the preprint in perpetuity. It is made available under aCC-BY-ND 4.0 International license.

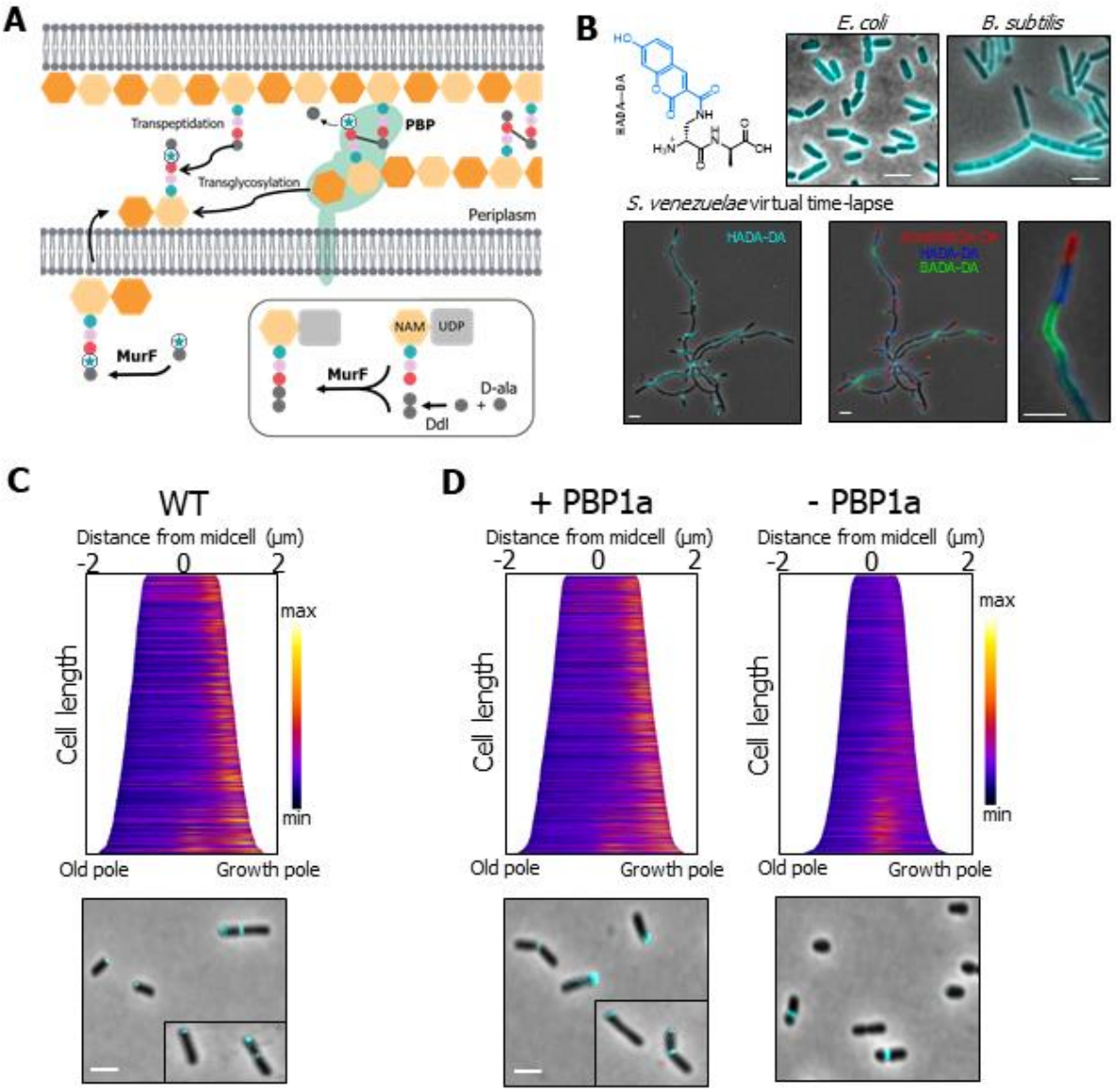

Figure 3. **Fluorescent D-amino acid dipeptide (FDAAD) labeling is absent from the growth pole in the PBP1 depletion**. (**A**) Schematic of the incorporation pathway of **f**luorescent **D**-**a**mino **a**cid **di**peptides (FDAADs), which are incorporated into the muropeptide precursor molecule in the cytoplasm by MurF ligase. The modified muropeptide precursor is flipped across the membrane and the activity of a bifunctional PBP crosslinks the new PG monomer into the existing PG sacculus. (**B**) Top row: structure of the FDAAD HADA—DA and merged phase and fluorescent channels of labeling patterns of HADA—DA in *E.coli* and *B. subtilis*. Bottom row: short pulse labeling of *S. venezuelae* sequentially labeled first with BADA—DA, followed by HADA—DA and Atto610DA—DA. (**C**) Demographs of wild-type (WT) cells depict incorporation of FDAADs at a population level. Median profiles of the fluorescence channel are stacked and ordered by cell length n = 513. (**D**) Demographs depict incorporation of FDAAD in the PBP1a depletion strain grown in the presence or absence of IPTG labeled + PBP1a and - PBP1a, respectively. Merged phase and fluorescent channels of cells with representative polar and septum labeling of FDAAD are shown to the right of each demograph. Scale bars: 2 μm. n = > 1000 per strain

bioRxiv preprint doi: https://doi.org/10.1101/2021.03.31.437934; this version posted March 31, 2021. The copyright holder for this preprint (which was not certified by peer review) is the author/funder, who has granted bioRxiv a license to display the preprint in perpetuity. It is made available under aCC-BY-ND 4.0 International license.

PBP1a is the major synthase incorporating PG at the pole

A. tumefaciens was labeled for ~5% of the cell cycle with HADA—DA. As expected, cells exhibit labeling at the growth pole during elongation, and at the septum in cells undergoing cell division (Figure 3C). This pole-to-septum labeling pattern is consistent with other cell wall labeling methods including fluorescent D-amino acids (FDAAs) [41] and D-cysteine labeling [1]. Similar to wild-type cells, a pole-to-septum labeling pattern was observed in the Δ3pbp mutant, consistent with a limited role for these class A PBPs in polar growth under the conditions tested (Supplementary Figure 3).

In stark contrast to wild-type (Figure 3C) or PBP1a replete cells (Figure 3D), pole-specific labeling with HADA—DA was almost completely absent from cells depleted of PBP1a for 20 hours (Figure 3D). Similar results were observed with NADA—DA and BADA—DA (Supplemental Figure 4A, B). Consistent with these observations, we tracked the growth of PBP1a-depleted cells for seven generations using a microfluidic device and found that the reduction in cell length occurred first for the new pole daughter cell and likely resulted from the loss of polar PG insertion by PBP1a (Supplemental Figure 3A, Supplemental movie 2). We thus concluded that PBP1a is the major PG synthase required for polar PG incorporation. Notably, PBP1a-depleted cells have more robust FDAAD labeling at the septum (Figure 3D), suggesting that additional glycosyltransferase enzymes remain active at the site of cell division.

bioRxiv preprint doi: https://doi.org/10.1101/2021.03.31.437934; this version posted March 31, 2021. The copyright holder for this preprint (which was not certified by peer review) is the author/funder, who has granted bioRxiv a license to display the preprint in perpetuity. It is made available under aCC-BY-ND 4.0 International license.

LD-transpeptidases contribute to growth-independent and growth-dependent PG modification

In contrast to FDAAD incorporation, which is linked to the PG precursors in the cytoplasm, the more conventional fluorescent D-amino acid (FDAA) labeling occurs in the periplasm through either DD-transpeptidase reactions carried out by PBPs or LD-transpeptidase reactions carried out by LDTs [41, 42]. As expected, wild-type and Δ3pbp cells labeled with a short pulse of the FDAA probe HADA show the characteristic pole-to-septum labeling pattern that is typical of *A. tumefaciens* growth (Figure 4A, Supplementary Figure 3). Notably, FDAADs label discrete regions at the pole and midcell, while FDAA labeling is more prominent in the sidewalls, particularly of the new pole compartment prior to cell division, while the old pole remains unlabeled. (Figure 4A white arrow). This labeling pattern is consistent with the reported growth-independent incorporation of FDAAs by LDTs [6]. Interestingly, we observed that a majority of growth-independent labeling occurred preferentially in the new pole compartment. To further support this idea, we labeled *A. tumefaciens* for 60 minutes with either HADA or HADA—DA and compared the labelling pattens (Supplemental figure 5). After a 60-minute incubation, HADA—DA labeling was primarily found in distinct regions at the pole and midcell, with little sidewall labeling, similar to a short pulse and consistent with areas of new synthesis. In contrast, the HADA labelling was much brighter, and fully labeled the sidewalls. HADA labeling was particularly enriched along the sidewalls of the new-pole compartment. Our observations during short and long-pulse labeling experiments suggests that, in addition to growth-dependent pole and midcell labeling,

bioRxiv preprint doi: https://doi.org/10.1101/2021.03.31.437934; this version posted March 31, 2021. The copyright holder for this preprint (which was not certified by peer review) is the author/funder, who has granted bioRxiv a license to display the preprint in perpetuity. It is made available under aCC-BY-ND 4.0 International license.

LDTs contribute to spatially distinct crosslinking of the cell wall, particularly along the sidewalls of the new pole daughter cell.

We next sought to test whether FDAA labeling at the growth pole was absent in the PBP1a depletion strain. In contrast to the absence of polar incorporation that was seen following FDAAD labeling, cells depleted of PBP1a labeled robustly at the growth pole with HADA (Figure 4A). Since PBP-mediated incorporation of FDAADs is absent from the growth pole in the PBP1a depletion (Figure 3D, Supplemental Figure 4A, B), the major enzymes incorporating HADA at the pole are most likely LDTs, consistent with recent findings for incorporation of FDAAs in *E. coli* [42]. Additionally, the activity of LDTs has been shown to be functionally linked to the activity of class A PBPs [42, 43]. Therefore, our findings indicate that LD-transpeptidation contributes to PG crosslinking at the growth pole.

bioRxiv preprint doi: https://doi.org/10.1101/2021.03.31.437934; this version posted March 31, 2021. The copyright holder for this preprint (which was not certified by peer review) is the author/funder, who has granted bioRxiv a license to display the preprint in perpetuity. It is made available under aCC-BY-ND 4.0 International license.

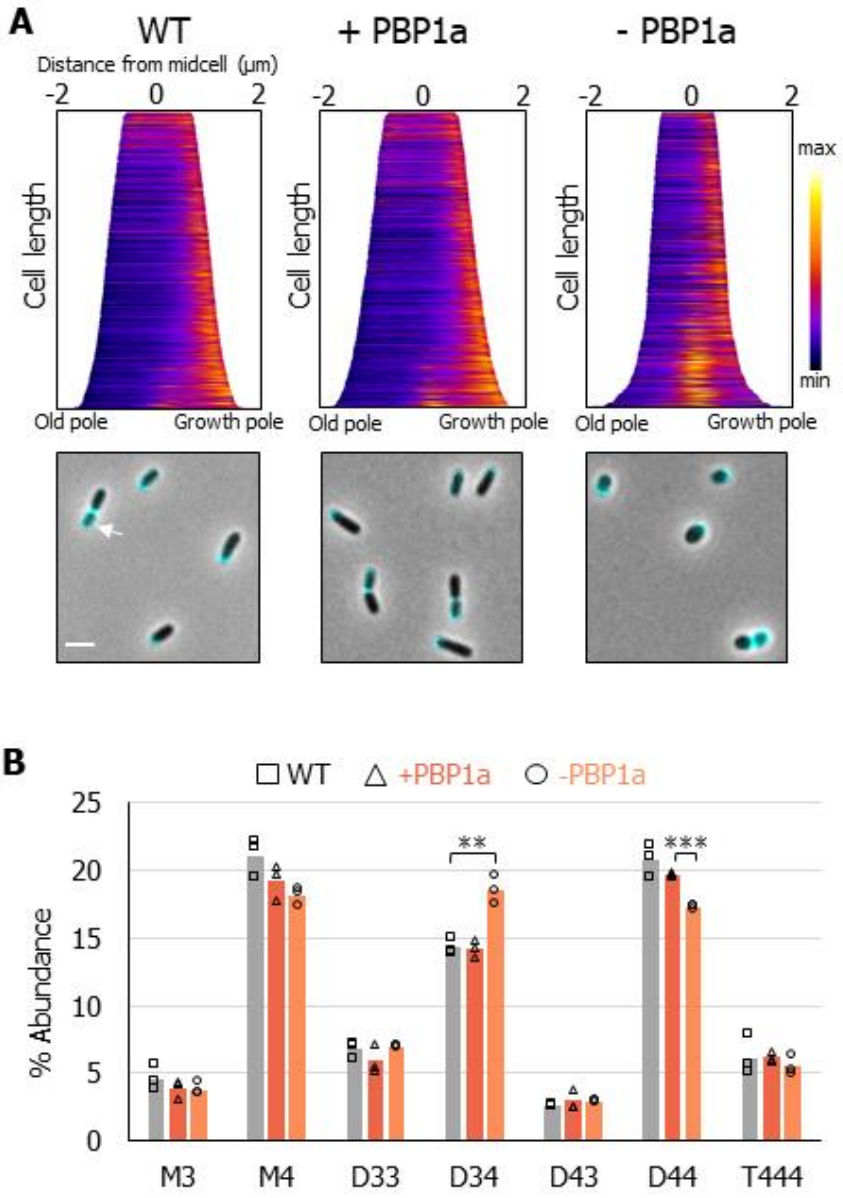

318

319 **Figure 4**. **Fluorescent D-amino acid (FDAA) and PG composition analysis illustrates a role for**
320 **LDTs in polar growth.** (**A**) Demographs of wildtype (WT) and the PBP1a depletion strain grown in the
321 presence or absence of IPTG labeled + PBP1a and - PBP1a, respectively. Demographs depict
322 incorporation of FDAA at a population level. Median profiles of the fluorescence channel are stacked and
323 ordered by cell length wildtype n = > 600 per strain. Merged phase and fluorescent channels of cells with
324 representative polar and septum labeling by FDAAs are shown below each demograph. Scale bar: 2 µm.
325 (**B**) Bar graphs depicting the average abundance of muropeptides obtained by UPLC analysis from
326 wildtype, and the PBP1a depletion strain grown in the presence or absence of IPTG for 16 hours. Major
327 muropeptides are labeled M, monomers; D, dimers; and T, trimers. Numbers indicate the length of the
328 muropeptide stems and the position of cross-links in dimers and trimers. Data shown are averages taken
329 from analysis of three independent biological samples. Samples that are statistically significant are
330 indicated (One-Way ANOVA with Tukey's multiple comparison test, ** $p<0.005$, *** $p<0.0005$). p-value
331 between + PBP1a and - PBP1a for D34 was 0.0588 and between WT and - PBP1a for D44 was 0.072.

332

bioRxiv preprint doi: https://doi.org/10.1101/2021.03.31.437934; this version posted March 31, 2021. The copyright holder for this preprint (which was not certified by peer review) is the author/funder, who has granted bioRxiv a license to display the preprint in perpetuity. It is made available under aCC-BY-ND 4.0 International license.

Depletion of PBP1a or loss of PBP1b2 leads to increased levels of LD-crosslinks in PG

Since depletion of PBP1a led to dramatic reduction in the polar incorporation of FDAADs, while maintaining polar FDAA incorporation we hypothesized that a decrease in the activity of PBPs relative to LDTs may lead to altered PG composition. We grew the PBP1a depletion strain in the presence or absence of IPTG for 16 hours, collected the cell wall fraction, and analyzed muropeptides by ultra-performance liquid chromatography (UPLC). The major muropeptides found in wild-type *A. tumefaciens* PG, included monomeric (M), dimeric (D) and trimeric (T) muropeptides (Figure 4B). PG from PBP1a-depleted cells had significantly reduced levels of muropeptides with DD-crosslinks, as seen by the ~3% reduction in D44 abundance (Figure 4B). As expected, this observation confirmed that depleting PBP1a leads to decreased DD-transpeptidase activity. Depletion of PBP1a also resulted in an increase in muropeptides containing LD-crosslinks, as indicated by the ~4% increase in D34 abundance (Figure 4B). A similar decrease in D44 abundance and increase in D34 abundance was also observed in the Δ*pbp1b2* (Supplemental Figure 4A), but not in the single deletions of *pbp1b1*, *pbp1c*, *pbp3a* or *pbp3b* (Supplemental Figure 4B). Therefore, the compositional changes in the double and triple mutant strain could likely be attributed to the deletion of *pbp1b2*. These results implicate PBP1b2 as an important DD-transpeptidase enzyme in *A. tumefaciens* and suggest that increased LDT activity may be a general response to decreased DD-transpeptidase levels, and not necessarily a specific response to depletion of PBP1a. Furthermore, since we saw an increase in muropeptide D34 but not D33 (Figure 4B), we hypothesize that decreased DD-transpeptidase levels activate only

bioRxiv preprint doi: https://doi.org/10.1101/2021.03.31.437934; this version posted March 31, 2021. The copyright holder for this preprint (which was not certified by peer review) is the author/funder, who has granted bioRxiv a license to display the preprint in perpetuity. It is made available under aCC-BY-ND 4.0 International license.

a subset of LDTs, and that another group of LDTs may function along with PBP1a during polar growth, consistent with the observation of HADA labeling at the growth pole.

Faropenem treatment inhibits polar growth in the Rhizobiales

Since species in the Rhizobiales have a large number of LD-transpeptidase enzymes (*A. tumefaceins* encodes 14 LDTs), deleting them all is a significant undertaking. β-lactam antibiotics are one of the most widely used classes of antibiotics that target cell wall synthesis enzymes, and these have been primarily studied for their ability to target PBPs [44]. A subclass of β-lactam antibiotics known as the carbapenems, including the penem antibiotic faropenem, are, however, useful for probing the activity of LDTs [45, 46]. Therefore, to characterize the global contribution of LDT activity during *A. tumefaciens* growth, we investigated the effect of five carbapenem antibiotics and one penem antibiotic on cell growth and morphology. In *A. tumefaciens*, we find that treatment with meropenem or faropenem leads to an overall decrease in PG crosslinkage, including both LD- and DD-crosslinks (Figure 5A, Supplemental Figure 5), suggesting that the targets of these drugs impact cell wall biosynthesis.

bioRxiv preprint doi: https://doi.org/10.1101/2021.03.31.437934; this version posted March 31, 2021. The copyright holder for this preprint (which was not certified by peer review) is the author/funder, who has granted bioRxiv a license to display the preprint in perpetuity. It is made available under aCC-BY-ND 4.0 International license.

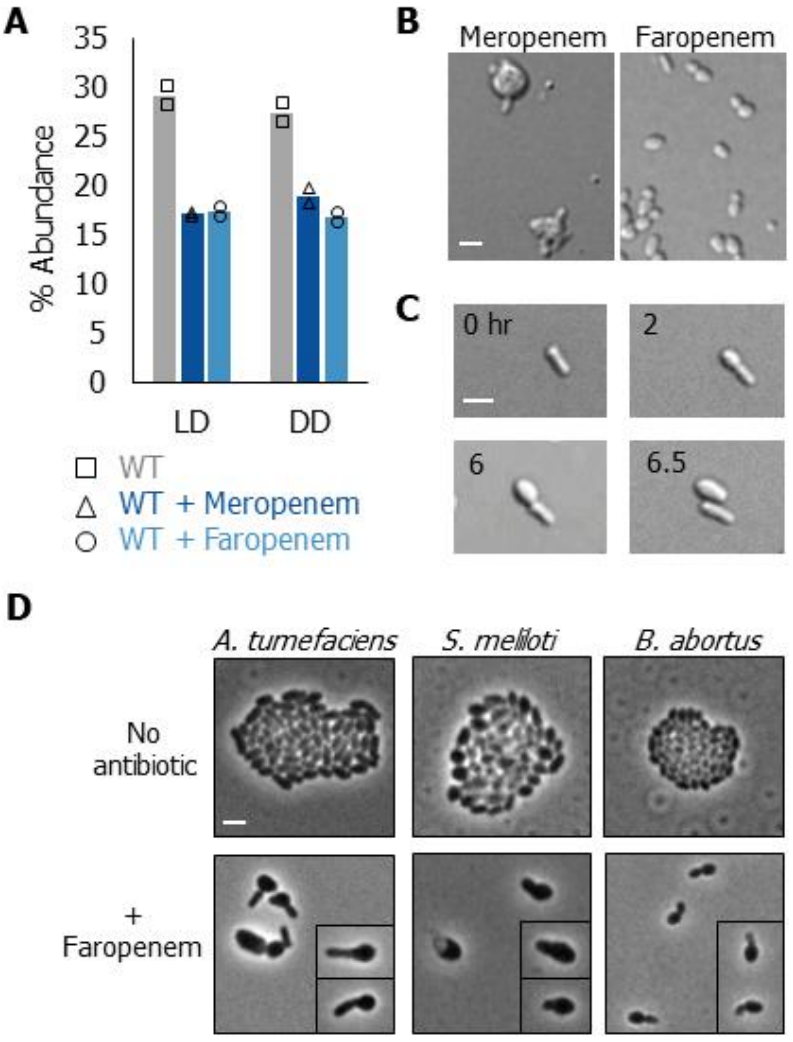

373

374 **Figure 5**. **Phenotypic characterization of carbapenem and penem antibiotic treatments.** (**A**)
375 Abundance of total LD- and DD-crosslinkages in PG isolated from wild-type cells, wild-type cells grown in
376 the presence of 1.5 µg/mL meropenem for 4 hours, and wild-type cells grown in the presence of 1.5
377 µg/mL of faropenem for 6 hours. Timepoints were chosen based on the onset of phenotypic changes.
378 Data shown are the total abundance of the muropeptides containing LD- or DD-crosslinks from analysis of
379 two independent samples. (**B**) Representative images of wild-type cells grown in the presence of 1.5
380 µg/mL meropenem and faropenem. Cells were incubated with antibiotics for 24 hours, then spotted on a
381 1% agarose pad and imaged using DIC microscopy. Scale bar: 2 µm (**C**) Time-lapse microscopy of wild-
382 type cells spotted on a 1% ATGN agarose pad supplemented with 1.5 µg/mL of faropenem; images were
383 acquired every 10 minutes. Indicated time in hours is shown. Scale bar: 2 µm (**D**) Representative phase
384 microscopy images of *A. tumefaciens*, *S. meliloti*, or *B. abortus* grown overnight in ATGN, Tryptone-Yeast
385 (TY) Extract or Brucella Broth, respectively, to an OD_{600} of 0.6 and spotted on a 1% ATGN agarose pad
386 with or without 1.5 µg/mL faropenem. Cells were imaged after 16 hours of growth. Scale bar: 2 µm.

387

bioRxiv preprint doi: https://doi.org/10.1101/2021.03.31.437934; this version posted March 31, 2021. The copyright holder for this preprint (which was not certified by peer review) is the author/funder, who has granted bioRxiv a license to display the preprint in perpetuity. It is made available under aCC-BY-ND 4.0 International license.

To better understand the impacts of these antibiotics, we observed morphological changes induced by drug treatment. Treatment with sub-minimum inhibitory concentrations (MIC) treatments with any of five carbapenem antibiotics: meropenem, imipenem, doripenem, ertapenem, or tebipenem for 24 hours induced mid-cell swelling (Figure 5B, Supplementary Figure 6). These data indicated that these carbapenem antibiotics may target an enzyme(s) with a specific role at the septum during cell division. Interestingly, faropenem-treated cells became wider and rounder after 24-hour exposure (Figure 5A), which pointed to the cellular target of faropenem as being important for the maintenance of rod shape during polar growth. In agreement, time-lapse microscopy of faropenem-treated cells revealed a loss of rod shape preferentially in the daughter compartment. Remarkably, following cell division the daughter cell which inherits the growth pole is large and round whereas the daughter cell inheriting the old growth pole retains its rod shape (Figure 5B, Supplemental movie 3). This phenotype was distinct from that associated with the treatment of the other carbapenem antibiotics and indicated that the cellular target(s) of faropenem was important to maintain proper PG integrity in the growth pole compartment.

The phenotype of faropenem-treated cells, along with the growth-independent labelling of HADA along the sidewalls of the new pole (Supplemental figure 6) suggested that the old and new cell compartments may have a distinct repertoire of PG synthesis enzymes that help to confer polar identity between the daughter cells. To determine if the cellular target(s) of faropenem were conserved in other Rhizobiales we treated the closely related plant symbiont *S. meliloti* and the obligate intracellular pathogen *B. abortus* with

bioRxiv preprint doi: https://doi.org/10.1101/2021.03.31.437934; this version posted March 31, 2021. The copyright holder for this preprint (which was not certified by peer review) is the author/funder, who has granted bioRxiv a license to display the preprint in perpetuity. It is made available under aCC-BY-ND 4.0 International license.

411 sub-lethal concentrations of faropenem. We observed swelling of the growth pole in *A.*
412 *tumefaciens, S. meliloti,* and *B. abortus* (Figure 5D). Thus, we have identified the β-
413 lactam antibiotic faropenem as a specific antibiotic inhibitor of polar growth among the
414 Rhizobiales. Altogether, these data suggest that cell wall enzymes that are important for
415 polar growth have a conserved role in agriculturally and medially important species of
416 Rhizobiales.

417

418 **The essentiality of PBP1a is conserved among the Rhizobiales**

419 Since faropenem targeting of the growth pole machinery is conserved, we sought to
420 determine if the essential role of PBP1a is also conserved in other Rhizobiales. We found
421 that treatment of *B. abortus* with the PBP1a-specific GTase inhibitor flavomycin
422 (moenomycin) [47] led to growth arrest and the formation of large, round cells (Figure
423 6B). Consistent with our findings that treatment of *B. abortus* with the PBP1a inhibitor
424 flavomycin causes cells to lose their rod-shape, a transposon mutagenesis screen of *B.*
425 *abortus* predicted that out of the bifunctional PBPs, only PBP1a may be essential for
426 growth [48]. In line with this, Bandara and colleagues were unable to obtain a PBP1a
427 mutant in *Brucella melitensis*, indicating that PBP1a is likely essential for viability [49].

bioRxiv preprint doi: https://doi.org/10.1101/2021.03.31.437934; this version posted March 31, 2021. The copyright holder for this preprint (which was not certified by peer review) is the author/funder, who has granted bioRxiv a license to display the preprint in perpetuity. It is made available under aCC-BY-ND 4.0 International license.

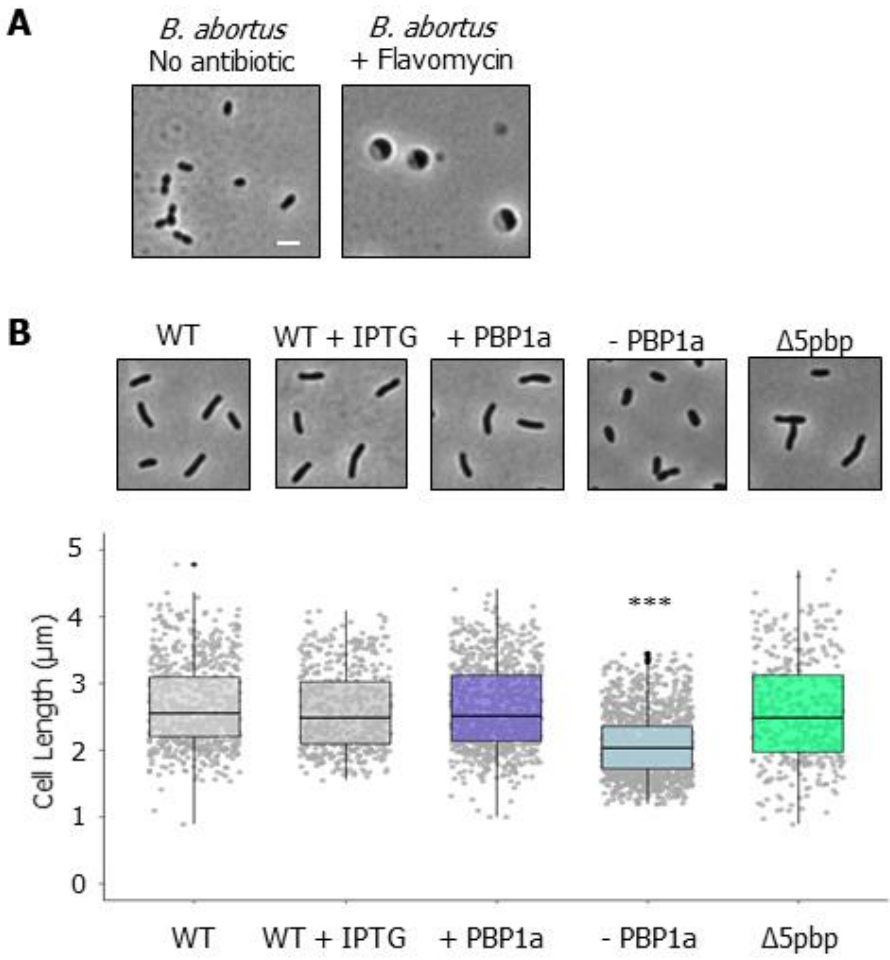

Figure 6. **Mechanisms of polar growth are conserved in the Rhizobiales *Brucella* and *Sinorhizobium*.**(**A**) Representative phase microscopy images of *B. abortus* grown overnight without antibiotic, with 20 µg/mL of flavomycin, or with 1.5 µg/mL of faropenem, after 16 hours cells were spotted on a 1% Brucella Broth agarose pad and imaged. (**B**) Top panel: phase microscopy images showing the phenotypes of *S. meliloti* wildtype (WT) and PBP mutants. Each strain was grown to exponential phase, spotted on a 1% TY agarose pad, and imaged by phase microscopy. Bottom panel: cell length distributions of PG synthase mutants. The indicated strains were grown to exponential phase, spotted on an agarose pad, imaged by phase microscopy, and subjected to cell lengths measurements using MicrobeJ [24]. The data are shown as box plots in the style of Tukey [25]. Distributions of cells significantly different from wildtype are indicated (***; One-Way ANOVA with Bonferroni correction, p< 2*10^16). n = >400 per strain.

bioRxiv preprint doi: https://doi.org/10.1101/2021.03.31.437934; this version posted March 31, 2021. The copyright holder for this preprint (which was not certified by peer review) is the author/funder, who has granted bioRxiv a license to display the preprint in perpetuity. It is made available under aCC-BY-ND 4.0 International license.

Next, we explored the function of PBPs in the closely related plant symbiont *S. meliloti.* *S. meliloti* encodes six bifunctional PBP homologs, including one PBP1a homolog, four PBP1b homologs, and one PBP1c homolog. We constructed a Δ5pbp mutant, which is lacking all four PBP1b homologs and the PBP1c homolog. The Δ5pbp mutant had a median cell length similar to that of wild-type *S. meliloti*, but with a slightly broader distribution of cell lengths, with ~88% of cells falling between 1.5 and 4 µm compared to ~97% of WT cells falling between these cell lengths. Interestingly, the Δ5pbp mutant retained its rod shape, similar to the Δ3pbp mutant of *A. tumefaciens*, suggesting that these enzymes contribute minimally to sustaining proper rod shape under standard growth conditions.

Similar to our findings for *A. tumefaciens*, we were unable to make a deletion of *pbp1a*, so we constructed a PBP1a depletion strain. Depletion of PBP1a led to a severe viability defect (Supplementary Figure 7A) and cells became shorter (Figure 6B) and wider (Supplementary Figure 7B). Thus, PBP1a is essential for polar growth and maintenance of proper rod shape in both *S. meliloti* and *A. tumefaciens*. Taken together, our data from *B. abortus*, *S. meliloti* and *A. tumefaciens* support the notion that PBP1a plays an essential and conserved role in polar growth among the Rhizobiales.

DISCUSSION

Bacteria employ widely diverse growth strategies. Unipolar growth, or incorporation of new cell wall material at a single pole, is a shared mode of growth among the

bioRxiv preprint doi: https://doi.org/10.1101/2021.03.31.437934; this version posted March 31, 2021. The copyright holder for this preprint (which was not certified by peer review) is the author/funder, who has granted bioRxiv a license to display the preprint in perpetuity. It is made available under aCC-BY-ND 4.0 International license.

Rhizobiales, but the mechanisms that drive polar PG insertion remain poorly understood. Most bacteria have multiple class A PBPs with semi-redundant functions and growth is supported by the presence of any one of the PBPs [50] In *C. crescentus*, four class A PBPs can support growth when expressed alone. [51] In *B. subtilis*, all 4 class A PBPs are dispensable and the SEDS protein RodA has likely taken over the essential function of the class A PBPs during elongation [52] In contrast, here we identified the class A PBP1a homolog as an essential protein needed to synthesize PG at the growth pole in *A. tumefaciens* and related genera, despite the presence of other class A PBPs. Current findings support the proposal that in laterally growing bacterial species, PBP1a homologs act as autonomous entities involved in PG remodeling or repair and do not function as a part of the core elongasome [15, 16]. Instead, the monofunctional glycosyltransferase RodA and the monofunctional transpeptidase PBP2 are required to maintain rod-shape [10, 53]. In contrast, we find that in the Rhizobiales, which lack MreB, RodA and PBP2 homologs, the bifunctional enzyme PBP1a is an essential core component of the elongasome of polar growing Rhizobiales. Loss of class A PBPs in *E. coli* or *B. subtilis* led to a decrease in cell width [54, 55]. Conversely, depletion of PBP1a in *A. tumefaciens* and *S. meliloti* led to a significant decrease in cell length and an increase in cell width (Figure 1B, C, Supplementary Figure 1B). This indicates that cells lacking PBP1a have a shorter period of cell elongation, and as a result, likely spend more time synthesizing the septum (Figure 3C, Supplementary Figure 3A, B). Thus, the regulation of PG synthesis that governs cell length and cell width in the Rhizobiales utilizes a novel mechanism compared to well-studied model bacteria. Perhaps because class A PBPs function independently of cytoskeletal

bioRxiv preprint doi: https://doi.org/10.1101/2021.03.31.437934; this version posted March 31, 2021. The copyright holder for this preprint (which was not certified by peer review) is the author/funder, who has granted bioRxiv a license to display the preprint in perpetuity. It is made available under aCC-BY-ND 4.0 International license.

complexes [10], PBP1a was freely available to assume the role of the primary enzyme driving polar PG synthesis prior to the loss of the *mre* operon. Notably, the other bifunctional PBPs minimally contributed to the maintenance of proper rod shape under the conditions tested in *A. tumefaciens* and *S. meliloti*. However, it is likely that the additional class A PBPs may make dedicated contributions under specific growth conditions. For example, in *E. coli*, PBP1a homologs are required for optimal growth in alkaline pH, while PBP1b homologs are required under acidic conditions [56]. Since the plant rhizosphere is an acidic environment [57], it is possible that the remaining bifunctional PBPs have specialized functions to maintain growth when bacteria are associated with a plant host. Additionally, duplication of the monofunctional PBP3 homolog among the Rhizobiales is restricted to a few species that interact with plants, suggesting this is not a broad solution to the loss of PBP2, but that PBP3b homologs may contribute more significantly to bacterial growth in plantae. In agreement with this idea, we found that of the two monofunctional PBP homologs (PBP3a and PBP3b), PBP3a - a clear homolog of the division-specific PBP3 - contributes to cell division, while deletion of *pbp3b* plays a minimal role in cell growth or cell shape under standard laboratory conditions but forms a synthetic lethal pair with PBP3a that functions in cell division.

In laterally growing bacterial species, the role of scaffolding PG synthase enzymes during elongation is fulfilled in part by the actin homolog MreB [58]. Homologs of MreBCD are absent in the Rhizobiales; thus, how PBP1a is recruited to the growth pole and how its activity is regulated remains unexplored. Recently, GPR (for Growth Pole

bioRxiv preprint doi: https://doi.org/10.1101/2021.03.31.437934; this version posted March 31, 2021. The copyright holder for this preprint (which was not certified by peer review) is the author/funder, who has granted bioRxiv a license to display the preprint in perpetuity. It is made available under aCC-BY-ND 4.0 International license.

509 Ring), a large (~226 kDa) apolipoprotein with similarity to the polar organizing protein
510 TipN from *C. crescentus*, was reported to form a ring at the growth pole in *A.*
511 *tumefaciens*, with depletion of this protein leading to rounded cells [59]. This phenotype
512 implicates GPR as a possible candidate to scaffold PG enzymes during elongation. In
513 addition, PG synthesis by PBP1a also requires hydrolysis of the existing sacculus to
514 allow for insertion of new muropeptides. A DD-endopeptidase (RgsM) that is predicted to
515 have hydrolysis activity was recently shown to be essential for polar growth in *S. meliloti*
516 [60], and thus represents an interesting candidate for polar PG hydrolysis.

517

518 Several lines of evidence suggest that FDAAs are primarily incorporated into the cell
519 wall through remodeling by LDTs [41, 42, 61, 62]. Cells depleted of PBP1a label
520 robustly at the growth pole with FDAAs, independently of PBP-mediated FDAAD
521 labeling. We also found that FDAAs label WT cells along the sidewalls of the new pole
522 much more brightly than the old pole. This points to a role for LDTs in not only polar
523 growth, but also sidewall remodeling of the new pole daughter cell (Figure 7).
524 Collectively, our results indicate that at the pole in *A. tumefaciens* FDAAD probes report
525 on nascent PG synthesis by PBP1a, whereas FDAAs are incorporated by the localized
526 activity of LD-transpeptidases on the bacterial cell surface. These findings demonstrate
527 the usefulness of FDAAD probes for distinguishing between growth-dependent, nascent
528 cell wall synthesis and growth-independent cell wall remodeling. In particular, the
529 growth pattern of species for which a high proportion of growth-independent remodeling
530 occurs can be obscured by FDAAs. Therefore, FDAADs are more useful in
531 distinguishing nascent PG synthesis mediated by PBPs.

bioRxiv preprint doi: https://doi.org/10.1101/2021.03.31.437934; this version posted March 31, 2021. The copyright holder for this preprint (which was not certified by peer review) is the author/funder, who has granted bioRxiv a license to display the preprint in perpetuity. It is made available under aCC-BY-ND 4.0 International license.

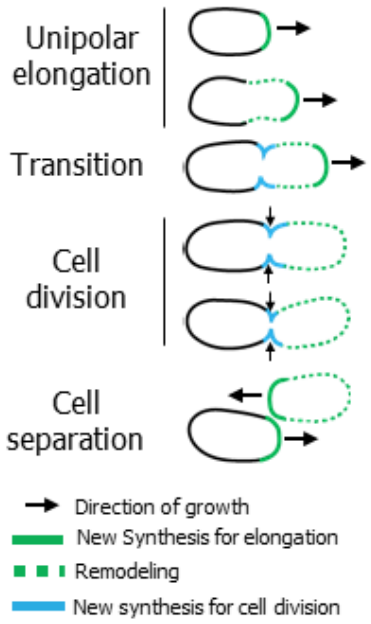

532

533 **Figure 7**. **Model of cell wall synthesis in the Rhizobiales. Unipolar elongation:** *A. tumefaceins*
534 elongates from a single pole using the action of an essential PBP1a homolog. As the cell gets longer, the
535 sidewalls of the new pole begin to be remodeled in a growth-independent manner, through the activity of
536 LD-transpeptidases. **Transition:** prior to cell division growth at the pole is terminated and growth at the
537 midcell is initiated, while remodeling of the new pole compartment continues. **Cell division:** during cell
538 division new PG is added at the midcell through the transpeptidase activity of two class B PBPs (with
539 PBP3a being the primary synthase) and the glycosyltransferase FtsW. **Cell separation:** after cell
540 separation, the new poles resume polar elongation from what was the site of cell division. Continuous
541 remodeling of the new pole daughter cell occurs throughout the cell cycle and is inherited into the new
542 pole daughter cell.

543

544

bioRxiv preprint doi: https://doi.org/10.1101/2021.03.31.437934; this version posted March 31, 2021. The copyright holder for this preprint (which was not certified by peer review) is the author/funder, who has granted bioRxiv a license to display the preprint in perpetuity. It is made available under aCC-BY-ND 4.0 International license.

Since LDTs are resistant to most classes of β-lactam antibiotics [63], crosslinking the cell wall via LDTs may contribute to the high antibiotic resistance to β-lactam antibiotics in the Rhizobiales. Here, we show that meropenem and faropenem inhibit LD- and DD-transpeptidation in *A. tumefaciens*, indicating that they may target LDTs and/or PBPs. Perhaps the loss of LDT activity disrupts the activity of high molecular weight PBPs if they function together in a growth pole complex. A combination of LDT and PBP-targeting antibiotics acted synergistically in killing *M. tuberculosis* [52], and a similar approach may also be effective against species in the Rhizobiales. Since faropenem causes swelling of the growth pole in *A. tumefacien*s, *S. meliloti* and *B. abortus* it is likely that the target(s) of this drug are conserved components of the growth machinery. Identification of the specific cellular target(s) of faropenem will provide candidate proteins for further characterization.

Expanding our understanding of the mechanism of polar growth in the Rhizobiales will help to shed light on the different strategies that can be employed by bacteria during cell elongation. Indeed, our findings highlight intriguing parallels with other, distantly related, polarly growing bacteria including the Actinobacteria. For example, PBP1a is essential in *Mycobacterium smegmatis* [64], an Actinobacteria that grows by bipolar elongation. In addition, PBP1a localizes to growth poles and is important for maintenance of rod shape in other Actinobacteria [65, 66]. Therefore, the reliance on PBP1a for synthesis of PG at the pole may be a key feature of polar-growing bacteria that arose independently in the Rhizobiales and Actinobacteria, indicating convergent evolution. Notably, the cell wall of polar-growing bacteria in both clades also contain a high proportion (~30-80%) of

bioRxiv preprint doi: https://doi.org/10.1101/2021.03.31.437934; this version posted March 31, 2021. The copyright holder for this preprint (which was not certified by peer review) is the author/funder, who has granted bioRxiv a license to display the preprint in perpetuity. It is made available under aCC-BY-ND 4.0 International license.

LDT-crosslinked PG [1, 67, 68], suggesting that LD-crosslinks may provide structural integrity. Furthermore, in *Mycobacterium* deletion of LDT-encoding genes leads to a loss of rod-shape [63], and LDTs also contribute to active PG synthesis of the sidewalls [37]. Finally, carbapenem antibiotics are routinely used to treat *M. tuberculosis* infections [20] hinting that the target of these drugs may be important in polar growing bacteria. Future work directed at characterizing the role of LDTs during polar growth in Rhizobiales and Actinobacteria is needed to determine if the high degree of LD-crosslinking is an innovation which allows for polar elongation to be adopted as the primary mode of growth. Overall, the possibility that there may be governing principles which allow for polar growth to emerge as a successful growth strategy is a fascinating concept which merits further study.

Acknowledgements

We thank Zachary Taylor, Edward Hall, and Srinivas Tekkam for synthesis of cell wall probes and Gyanu Lamichhane for the generous gift of the penem and carbapenem antibiotics. We thank members of Jerod Skyberg's lab for providing lab space and materials to work on *B. abortus*. We also thank members of the Brown lab and Marie Elliot for helpful discussions and critical reading of this manuscript. PB and MW were supported by the National Science Foundation, IOS1557806. MW was supported by the Life Sciences Fellowship at the University of Missouri. Research in the Cava lab (FC, AA) is supported by the Laboratory for Molecular Infection Medicine Sweden, the Knut and Alice Wallenberg Foundation, the Kempe Foundation and the Swedish Research Council. AA is supported by a MIMS/VR PhD position. EK was supported by the Life

bioRxiv preprint doi: https://doi.org/10.1101/2021.03.31.437934; this version posted March 31, 2021. The copyright holder for this preprint (which was not certified by peer review) is the author/funder, who has granted bioRxiv a license to display the preprint in perpetuity. It is made available under aCC-BY-ND 4.0 International license.

591 Sciences Research Foundation (LSRF) at the Harvard Medical School. AB received
592 funding from the German Research Foundation (Project 269423233 - TRR 174). NIH
593 grants R35GM122556 to YVB and GM113172 and to MSV and YVB and
594 R35GM136365 to MSV. YVB is also supported by a Canada 150 Research Chair in
595 Bacterial Cell Biology funded by the Canadian Institutes of Health Research.

596

597 **MATERIALS AND METHODS**

598 **Bacterial strains, plasmids, and growth conditions**. A list of all bacterial strains used
599 in this study is provided in Supplemental Table 1. *Agrobacterium tumefaciens* C58 and
600 derived strains were grown in ATGN minimal media [69] without exogenous iron at 28°C
601 with shaking. When appropriate, kanamycin (KAN) was used at the working
602 concentration of 300 µg/ml. When indicated, isopropyl β-D-1-thio-galactopyranoside
603 (IPTG) was used as an inducer at a concentration of 1 mM. *Sinorhizobium meliloti*
604 strains were grown in Tryptone-Yeast (TY) medium. When appropriate, KAN was used
605 at the working concentration of 100 µg/ml, Gentamicin (GM) was used as 20 µg/ml, and
606 IPTG was used at a concentration of 500 µg/ml. *Brucella abortus* strain S19 was grown
607 in brucella broth. *E. coli* strains were grown in Luria-Bertani medium at 37°C. For *E. coli*
608 DH5α and S17-1 λ *pir*, when appropriate 50 µg/ml or 30 µg/ml of KM, respectively, was
609 added.

610

611 **Construction of strains and plasmids.** A list of all primers used in this study is
612 provided in Supplemental Table 2. For amplification of target genes, primer names

bioRxiv preprint doi: https://doi.org/10.1101/2021.03.31.437934; this version posted March 31, 2021. The copyright holder for this preprint (which was not certified by peer review) is the author/funder, who has granted bioRxiv a license to display the preprint in perpetuity. It is made available under aCC-BY-ND 4.0 International license.

613 indicate the primer orientation and added restriction sites. All expression vectors were
614 verified by sequencing. All vectors were introduced into *A. tumefaciens* strains utilizing
615 standard electroporation protocols [70] with the addition of IPTG in the media when
616 introducing plasmids into depletion backgrounds.

617

618 **Construction of deletion/depletion plasmids and strains.** Vectors for gene deletion
619 by allelic exchange were constructed using recommended methods for *A. tumefaciens*
620 [70]. Briefly, 500-bp fragments upstream and 500 bp downstream of the target gene
621 were amplified using primer pairs P1/P2 and P3/4 respectively. Amplicons were spliced
622 together by SOEing using primer pair P1/P4. The amplicon was digested and ligated
623 into pNTPS139. The deletion plasmids were introduced into *A. tumefaciens* by mating
624 using an *E. coli* S17 conjugation strain to create KM resistant, sucrose sensitive primary
625 integrants. Primary integrants were grown overnight in media with no selection.
626 Secondary recombinants were screened by patching for sucrose resistance and KM
627 sensitivity. Colony PCR with primers P5/P6 for the respective gene target was used to
628 confirm deletion. PCR products from P5/P6 primer sets were sequenced to further
629 confirm deletions.

630 For depletion strain construction, target genes (*pbp1a* or *pbp3a*) were amplified,
631 digested and ligated into pUC18-mini-Tn*7*T-GM-P_{lac}. The mini-Tn*7* vector, along with
632 the pTNS3 helper plasmid, were introduced into C58Δ*tetRA*::a-*att*Tn*7* as described
633 previously [27]. Transformants were selected for GM resistance and insertion of the
634 target gene into the a-*att* site was verified by colony PCR using the tet forward and
635 Tn7R109 primer. PCR products were sequenced to confirm insertion of the correct

bioRxiv preprint doi: https://doi.org/10.1101/2021.03.31.437934; this version posted March 31, 2021. The copyright holder for this preprint (which was not certified by peer review) is the author/funder, who has granted bioRxiv a license to display the preprint in perpetuity. It is made available under aCC-BY-ND 4.0 International license.

gene. Next, the target gene was deleted from the native locus as described above in the presence of 1 mM IPTG to drive expression of the target gene from the engineered site.

To generate the *S. meliloti* strain lacking the five non-essential PBPs, the corresponding genes were consecutively deleted from the Rm2011 *rgsP-egfp* genome using the sucrose selection method. [71] To generate the *S. meliloti* MrcA1 depletion strain, first plasmid pK18mobsac-mrcA1del was integrated into the Rm2011 *rgsP-egfp* genome, then an ectopic *mrcA1* copy was introduced on plasmid pGCH14-mrcA1 followed by sucrose selection of mutant clones with deletion of the native *mrcA1* allele. The curable plasmid pGCH14, which is maintained in single copy in *S. meliloti* due to the replication operon *repABCpMlb_lacO*, prone to repression by LacI was used as vector to conditionally establish the ectopic copy of *mrcA1* under control of its native promoter. pSRKKm, carrying *lacI*, was introduced into the strain with chromosomal deletion of *mrcA1*, carrying pGCH14-mrcA1, and the resulting strain Rm2011 *rgsP-egfp* *mrcA1*^{dpl} was grown in presence of 500 µm IPTG. Growth in the absence of IPTG induced MrcA1 depletion due to loss of the ectopic *mrcA1* copy.

Phase and Fluorescence microscopy. A small volume (~1 µl) of cells in exponential phase (OD_{600} = 0.2 - 0.4) was applied to a 1% ATGN agarose pad as described previously [72]. DIC, Phase contrast and epifluorescence microscopy were performed with an inverted Nikon Eclipse TiE and a QImaging Rolera em-c2 123 1K EMCCD camera with Nikon Elements Imaging Software. For time-lapse microscopy, images were collected every ten minutes, unless otherwise stated.

bioRxiv preprint doi: https://doi.org/10.1101/2021.03.31.437934; this version posted March 31, 2021. The copyright holder for this preprint (which was not certified by peer review) is the author/funder, who has granted bioRxiv a license to display the preprint in perpetuity. It is made available under aCC-BY-ND 4.0 International license.

Quantification of cell length distributions. Cells were grown overnight in ATGN. Cells were diluted in ATGN to an OD_{600} = 0.2 and allowed to grow until reaching an OD_{600} = 0.4 - 0.6. Live cells were imaged using phase contrast microscopy and cell length distributions of the indicated number of cells per strain were determined using the longest medial axis as measured by MicrobeJ software [24].

Quantification of cell morphologies, FDAA and FDAAD labeling patterns. For *A. tumefaciens*, cells were grown overnight in ATGN media and diluted in the same conditions to an OD_{600} = 0.20 and allowed to grow until reaching an OD_{600} = 0.4 - 0.6. At this point cells were labeled with 1mM of the fluorescent-D-amino acid (FDAA) HCC-amino-D-alanine (HADA) or the fluorescent dipeptide (FDAAD) NBD-amino-D-alanine-D-alanine (HADA—DA) as previously described [36, 38, 41]. Immediately following a five-minute incubation, cells were ethanol fixed to prevent further growth. Phase contrast and epifluorescence microscopy was performed on the reported number of cells. For *E. coli*, cells were grown overnight at 37˚C in M9 + 0.2% glucose minimal medium and diluted in the same conditions to an OD_{600} = 0.1 and allowed to grow until reaching an OD_{600} = 0.4 - 0.6. At this point cells were labeled with 1 mM of HADA—DA. After an incubation of 90 minutes cells were ethanol fixed and washed 3 times in 1 mL PBS before imaging. For *B. subtilis 3610*, cells were grown overnight at 37˚C in S750 + 1% glucose defined minimal medium and diluted in the same conditions to an OD_{600} = 0.1 and allowed to grow until reaching an OD_{600} = 0.4 - 0.6. At this point cells were labeled with 5 mM of HADA—DA. After an incubation of 120 minutes cells were ethanol fixed and washed 3 times in 1 mL PBS before imaging. For *S. venezuelae*, cells were grown

bioRxiv preprint doi: https://doi.org/10.1101/2021.03.31.437934; this version posted March 31, 2021. The copyright holder for this preprint (which was not certified by peer review) is the author/funder, who has granted bioRxiv a license to display the preprint in perpetuity. It is made available under aCC-BY-ND 4.0 International license.

overnight at 30˚C in LB medium and diluted in the same conditions to an OD_{600} = 0.1 and allowed to grow until reaching an OD_{600} = 0.4 - 0.6. At this point cells were labeled with 1 mM BODIPY FL-amino-d-alaninyl-D-alanine (BADA—DA). After an incubation of 15 minutes, cells were washed once with 1 mL LB and resuspended in 500 uL LB containing 2 mM HADA—DA. After an incubation of 15 minutes, cells were washed once with 1 mL LB and resuspended in 500 uL LB containing 1 mM ATTO 610-amino-d-alaninyl-D-alanine (Atto610ADA—DA). After an incubation of 15 minutes cells were ethanol fixed and washed 3 times in 1 mL PBS before imaging.

Demographs were constructed using MicrobeJ. For demographs, cells were arranged from top to bottom according to their cell lengths and each cell was oriented such that the new pole (defined as the cell pole with the higher fluorescence intensity as determined by FDAA or FDAAD labeling or the smaller pole diameter in cells without label) was oriented to the right.

Synthesis of HADA—DA.

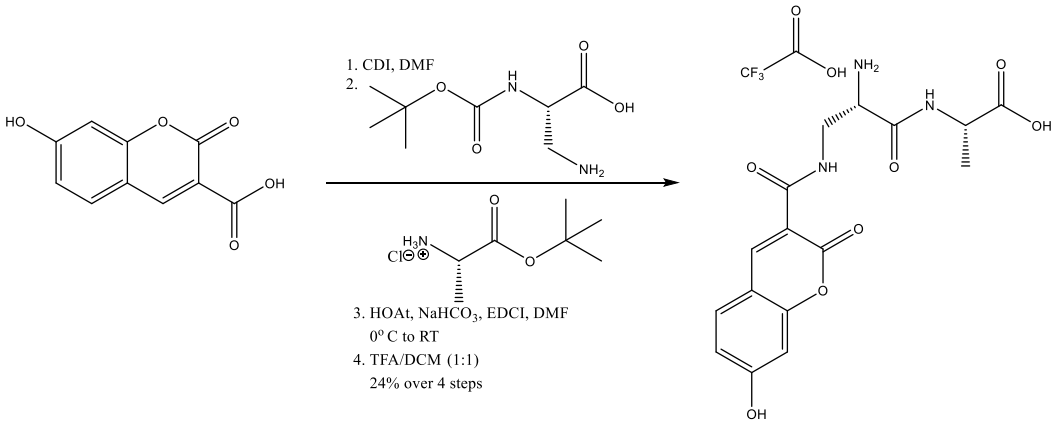

Molecular Weight: 363.32600

bioRxiv preprint doi: https://doi.org/10.1101/2021.03.31.437934; this version posted March 31, 2021. The copyright holder for this preprint (which was not certified by peer review) is the author/funder, who has granted bioRxiv a license to display the preprint in perpetuity. It is made available under aCC-BY-ND 4.0 International license.

A solution of 7-hydroxycoumarin-3-carboxylic acid (HCC) (105 mg, 0.51 mmol) and carbonyldiimidazole (83 mg, 0.51 mmol) in anhydrous DMF (5 mL) was stirred at room temperature (RT) for 2 h under an atmosphere of argon. Boc-D-2,3-diaminopropionic acid (104 mg, 0.51 mmol) was then added and the reaction mixture was allowed to stir at RT for 18 h. DMF was removed *in vacuo*. The residue was diluted with EtOAc (35 mL), washed with 1N HCl (20 mL) and water (30 mL). The combined aqueous layers are back-extracted with EtOAc (20 mL). The combined organic layers were washed with brine (20 mL), dried over sodium sulfate, filtered, and concentrated to dryness. The crude product was dissolved in anhydrous DMF. D-alanine tert-butyl ester hydrochloride (111 mg, 0.612 mmol), HOAt (83.5 mg, 0.612 mmol) and $NaHCO_3$ (94 mg, 1.12 mmol) were added successively, and the reaction mixture was cooled to 0 ^oC. EDCI (117 mg, 0.612 mmol) was then added, and the reaction mixture was stirred for 12 h. The solvent was removed in *vacuo* and the product was diluted with EtOAc, washed with 1N HCl, water, brine, dried over sodium sulfate, filtered and concentrated. The crude product was dissolved in DCM/TFA (1:1, 4 mL) mixture, stirred for 1 h and evaporated to dryness. The yellow color solid was dissolved in acetonitrile/water and purified by reverse phase HPLC and lyophilized to yield the desired product as a pale yellow solid (63 mg, 26 %). 1H NMR (500 MHz, DMSO-*d6*) 11.37 (br s, 1H), 8.91 (m, 1H), 8.90 (m, 1H), 8.81 (s, 1H), 8.42 (br s, 3H), 7.83 (m, 1H), 5.94 (m, 1H), 5.89 (s, 1H), 4.24 (m, 1H), 4.04 (br s, 1H), 3.77 (m, 1H), 3.68 (m, 1H), 1.32 (s, 1H); HRMS-ESI-TOF m/z calc C16H18N3O7 (M+H) 364.1145, Found 364.1161.

PG compositional analysis.

bioRxiv preprint doi: https://doi.org/10.1101/2021.03.31.437934; this version posted March 31, 2021. The copyright holder for this preprint (which was not certified by peer review) is the author/funder, who has granted bioRxiv a license to display the preprint in perpetuity. It is made available under aCC-BY-ND 4.0 International license.

For PG analysis, three cultures of each of strain were grown overnight in 3 ml culture tubes of ATGN minimal media at 28°C with shaking; the + PBP1a strain was supplemented with 1mM IPTG. The 3 ml cultures were then added to 50 ml flasks of fresh ATGN and allowed to grow under the same conditions until reaching an exponential phase OD_{600} of 0.5-0.6. Cells were then pelleted by centrifugation at 4000 x *g* for 10 minutes. Cell pellets were washed three times with ATGN by centrifugation and resuspension to remove IPTG. After the final wash, the 3 cell pellets from the + PBP1a strain were split and resuspended in 50 ml ATGN with or without IPTG. Each culture was grown for 16 hours (hr). to an OD_{600} of 0.6 After 146 h of growth, 50 ml of the exponential cultures were collected and pelleted by centrifugation at 4000 x *g* for 20 minutes. Cell pellets were resuspended in 3 mL of ATGN and 6 mL of 6% SDS and stirred with magnets while boiling for 4 h. Next, samples were removed from heat but continued to stir overnight. Samples were then shipped to Cava laboratory for purification and analysis. Upon arrival, cells were boiled and simultaneously stirred by magnets for 2 h. After 2 h, boiling was stopped, and samples were stirred overnight. PG was pelleted by centrifugation for 13 minutes (min) at 60,000 rpm (TLA100.3 Beckman rotor, Optima Max-TL ultracentrifuge; Beckman), and the pellets were washed 3 to 4 times by repeated cycles of centrifugation and resuspension in water. The pellet from the final wash was resuspended in 50 µl of 50 mM sodium phosphate buffer, pH 4.9, and digested overnight with 100 µg/ml of muramidase at 37°C. Muramidase digestion was stopped by boiling for 4 min. Coagulated protein was removed by centrifugation for 15 min at 15,000 rpm in a desktop microcentrifuge. The muropeptides were mixed with 15 µl 0.5 M sodium borate and subjected to reduction of muramic acid residues into

bioRxiv preprint doi: https://doi.org/10.1101/2021.03.31.437934; this version posted March 31, 2021. The copyright holder for this preprint (which was not certified by peer review) is the author/funder, who has granted bioRxiv a license to display the preprint in perpetuity. It is made available under aCC-BY-ND 4.0 International license.

747 muramitol by sodium borohydride (10 mg/ml final concentration, 20 min at room
748 temperature) treatment. Samples were adjusted to pH 3 to 4 with orthophosphoric acid
749 and filtered (0.2-µm filters). Analysis of muropeptides was performed on an ACQUITY
750 Ultra Performance Liquid Chromatography (UPLC) BEH C18 column, 130Å, 1.7 µm, 2.1
751 mm x 150 mm (Water, USA) and detected at Abs. 204 nm with ACQUITY UPLC UV-
752 visible detector. For data shown in Figure 4B and Supplementary Figure 7B,
753 muropeptides were separated with organic buffers at 45°C using a linear gradient from
754 buffer A (formic acid 0.1% (v/v) in water) to buffer B (formic acid 0.1% (v/v) in
755 acetonitrile) in a 18 minutes run with a 0.25 ml/min flow. For data shown in Figure 5A
756 and Supplementary Figure 5A, muropeptides were separated using a linear gradient
757 from buffer A (sodium phosphate buffer 50 mM pH 4.35) to buffer B (sodium phosphate
758 buffer 50 mM pH 4.95 methanol 15% (v/v)) with a flow of 0.25 mL/min in a 20 min run.
759 Individual muropeptides were quantified from their integrated areas using samples of
760 known concentration as standards. Muropeptide abundance was statistically compared
761 using a one-way ANOVA with Tukey's multiple comparisons test.

762

763 **REFERENCES**

764 1. Brown, P.J., et al., *Polar growth in the Alphaproteobacterial order Rhizobiales.*
765 Proc Natl Acad Sci U S A, 2012. **109**(5): p. 1697-701.
766 2. Batut, J., S.G. Andersson, and D. O'Callaghan, *The evolution of chronic infection*
767 *strategies in the alpha-proteobacteria.* Nat Rev Microbiol, 2004. **2**(12): p. 933-45.
768 3. Randich, A.M. and Y.V. Brun, *Molecular mechanisms for the evolution of*
769 *bacterial morphologies and growth modes.* Front Microbiol, 2015. **6**: p. 580.
770 4. Escobar, M.A. and A.M. Dandekar, *Agrobacterium tumefaciens as an agent of*
771 *disease.* Trends Plant Sci, 2003. **8**(8): p. 380-6.
772 5. Mansfield, J., et al., *Top 10 plant pathogenic bacteria in molecular plant*
773 *pathology.* Mol Plant Pathol, 2012. **13**(6): p. 614-29.

bioRxiv preprint doi: https://doi.org/10.1101/2021.03.31.437934; this version posted March 31, 2021. The copyright holder for this preprint (which was not certified by peer review) is the author/funder, who has granted bioRxiv a license to display the preprint in perpetuity. It is made available under aCC-BY-ND 4.0 International license.

6. Kuru, E., et al., *Mechanisms of Incorporation for D-Amino Acid Probes That Target Peptidoglycan Biosynthesis.* ACS Chem Biol, 2019. **14**(12): p. 2745-2756.
7. Vollmer, W. and U. Bertsche, *Murein (peptidoglycan) structure, architecture and biosynthesis in Escherichia coli.* Biochim Biophys Acta, 2008. **1778**(9): p. 1714-34.
8. Typas, A., et al., *From the regulation of peptidoglycan synthesis to bacterial growth and morphology.* Nat Rev Microbiol, 2011. **10**(2): p. 123-36.
9. Yoshida, H., et al., *Crystal structures of penicillin-binding protein 3 (PBP3) from methicillin-resistant Staphylococcus aureus in the apo and cefotaxime-bound forms.* J Mol Biol, 2012. **423**(3): p. 351-64.
10. Cho, H., et al., *Bacterial cell wall biogenesis is mediated by SEDS and PBP polymerase families functioning semi-autonomously.* Nat Microbiol, 2016. **1**: p. 16172.
11. Meeske, A.J., et al., *SEDS proteins are a widespread family of bacterial cell wall polymerases.* Nature, 2016. **537**(7622): p. 634-638.
12. Leclercq, S., et al., *Interplay between Penicillin-binding proteins and SEDS proteins promotes bacterial cell wall synthesis.* Scientific reports, 2017. **7**: p. 43306-43306.
13. Reichmann, N.T., et al., *SEDS-bPBP pairs direct lateral and septal peptidoglycan synthesis in Staphylococcus aureus.* Nat Microbiol, 2019. **4**(8): p. 1368-1377.
14. Sjodt, M., et al., *Structural coordination of polymerization and crosslinking by a SEDS-bPBP peptidoglycan synthase complex.* Nat Microbiol, 2020. **5**(6): p. 813-820.
15. Straume, D., et al., *Class A PBPs have a distinct and unique role in the construction of the pneumococcal cell wall.* Proc Natl Acad Sci U S A, 2020. **117**(11): p. 6129-6138.
16. Vigouroux, A., et al., *Class-A penicillin binding proteins do not contribute to cell shape but repair cell-wall defects.* Elife, 2020. **9**.
17. Cameron, T.A., et al., *Peptidoglycan synthesis machinery in Agrobacterium tumefaciens during unipolar growth and cell division.* mBio, 2014. **5**(3): p. e01219-14.
18. Gupta, R., et al., *The Mycobacterium tuberculosis protein LdtMt2 is a nonclassical transpeptidase required for virulence and resistance to amoxicillin.* Nat Med, 2010. **16**(4): p. 466-9.
19. Glauner, B., J.V. Holtje, and U. Schwarz, *The composition of the murein of Escherichia coli.* J Biol Chem, 1988. **263**(21): p. 10088-95.
20. Cordillot, M., et al., *In vitro cross-linking of Mycobacterium tuberculosis peptidoglycan by L,D-transpeptidases and inactivation of these enzymes by carbapenems.* Antimicrob Agents Chemother, 2013. **57**(12): p. 5940-5.
21. Kysela, D.T., et al., *Biological consequences and advantages of asymmetric bacterial growth.* Annu Rev Microbiol, 2013. **67**: p. 417-35.
22. Aldridge, B.B., et al., *Asymmetry and aging of mycobacterial cells lead to variable growth and antibiotic susceptibility.* Science, 2012. **335**(6064): p. 100-4.
23. Piovesan, D., et al., *MobiDB 3.0: more annotations for intrinsic disorder, conformational diversity and interactions in proteins.* Nucleic Acids Res, 2018. **46**(D1): p. D471-D476.

bioRxiv preprint doi: https://doi.org/10.1101/2021.03.31.437934; this version posted March 31, 2021. The copyright holder for this preprint (which was not certified by peer review) is the author/funder, who has granted bioRxiv a license to display the preprint in perpetuity. It is made available under aCC-BY-ND 4.0 International license.

24. Ducret, A., E.M. Quardokus, and Y.V. Brun, *MicrobeJ, a tool for high throughput bacterial cell detection and quantitative analysis.* Nat Microbiol, 2016. **1**(7): p. 16077.
25. McGill, R., J.W. Tukey, and W.A. Larsen, *Variations of Box Plots.* The American Statistician, 1978. **32**(1): p. 12-16.
26. Curtis, P.D. and Y.V. Brun, *Identification of essential alphaproteobacterial genes reveals operational variability in conserved developmental and cell cycle systems.* Mol Microbiol, 2014. **93**(4): p. 713-35.
27. Figueroa-Cuilan, W., et al., *Mini-Tn7 Insertion in an Artificial attTn7 Site Enables Depletion of the Essential Master Regulator CtrA in the Phytopathogen Agrobacterium tumefaciens.* Appl Environ Microbiol, 2016. **82**(16): p. 5015-25.
28. Derouaux, A., et al., *The monofunctional glycosyltransferase of Escherichia coli localizes to the cell division site and interacts with penicillin-binding protein 3, FtsW, and FtsN.* J Bacteriol, 2008. **190**(5): p. 1831-4.
29. Di Berardino, M., et al., *The monofunctional glycosyltransferase of Escherichia coli is a member of a new class of peptidoglycan-synthesising enzymes.* FEBS Lett, 1996. **392**(2): p. 184-8.
30. Cserti, E., et al., *Dynamics of the peptidoglycan biosynthetic machinery in the stalked budding bacterium Hyphomonas neptunium.* Mol Microbiol, 2017. **103**(5): p. 875-895.
31. Miyakawa, T., et al., *Cell wall peptidoglycan mutants of Escherichia coli K-12: existence of two clusters of genes, mra and mrb, for cell wall peptidoglycan biosynthesis.* J Bacteriol, 1972. **112**(2): p. 950-8.
32. Howell, M., et al., *Agrobacterium tumefaciens divisome proteins regulate the transition from polar growth to cell division.* Mol Microbiol, 2019. **111**(4): p. 1074-1092.
33. Fujiwara, T. and S. Fukui, *Unidirectional growth and branch formation of a morphological mutant, Agrobacterium tumefaciens.* J Bacteriol, 1974. **120**(2): p. 583-9.
34. Taguchi, A., et al., *FtsW is a peptidoglycan polymerase that is functional only in complex with its cognate penicillin-binding protein.* Nature microbiology, 2019. **4**(4): p. 587-594.
35. Radkov, A.D., et al., *Imaging Bacterial Cell Wall Biosynthesis.* Annu Rev Biochem, 2018. **87**: p. 991-1014.
36. Liechti, G.W., et al., *A new metabolic cell-wall labelling method reveals peptidoglycan in Chlamydia trachomatis.* Nature, 2014. **506**(7489): p. 507-510.
37. Garcia-Heredia, A., et al., *Peptidoglycan precursor synthesis along the sidewall of pole-growing mycobacteria.* Elife, 2018. **7**.
38. Kuru, E., *NOVEL WAYS FOR DECORATING BACTERIAL CELL WALLS ADVANCE FUNDAMENTAL KNOWLEDGE ABOUT BACTERIAL GROWTH*. 2016, Indiana University: ProQuest LLC.
39. Hsu, Y.P., et al., *Full color palette of fluorescent d-amino acids for in situ labeling of bacterial cell walls.* Chem Sci, 2017. **8**(9): p. 6313-6321.
40. Kuru, E., et al., *Synthesis of fluorescent D-amino acids and their use for probing peptidoglycan synthesis and bacterial growth in situ.* Nat Protoc, 2015. **10**(1): p. 33-52.

bioRxiv preprint doi: https://doi.org/10.1101/2021.03.31.437934; this version posted March 31, 2021. The copyright holder for this preprint (which was not certified by peer review) is the author/funder, who has granted bioRxiv a license to display the preprint in perpetuity. It is made available under aCC-BY-ND 4.0 International license.

41. Kuru, E., et al., *In Situ probing of newly synthesized peptidoglycan in live bacteria with fluorescent D-amino acids.* Angew Chem Int Ed Engl, 2012. **51**(50): p. 12519-23.
42. Montón Silva, A., et al., *The Fluorescent D-Amino Acid NADA as a Tool to Study the Conditional Activity of Transpeptidases in Escherichia coli.* 2018. **9**(2101).
43. Hugonnet, J.E., et al., *Factors essential for L,D-transpeptidase-mediated peptidoglycan cross-linking and beta-lactam resistance in Escherichia coli.* Elife, 2016. **5**.
44. Tooke, C.L., et al., *beta-Lactamases and beta-Lactamase Inhibitors in the 21st Century.* J Mol Biol, 2019. **431**(18): p. 3472-3500.
45. Kumar, P., et al., *Mycobacterium abscessus l,d-Transpeptidases Are Susceptible to Inactivation by Carbapenems and Cephalosporins but Not Penicillins.* Antimicrob Agents Chemother, 2017. **61**(10).
46. Kumar, P., et al., *Non-classical transpeptidases yield insight into new antibacterials.* Nat Chem Biol, 2017. **13**(1): p. 54-61.
47. Gampe, C.M., et al., *Modular synthesis of diphospholipid oligosaccharide fragments of the bacterial cell wall and their use to study the mechanism of moenomycin and other antibiotics.* Tetrahedron, 2011. **67**(51): p. 9771-9778.
48. Sternon, J.F., et al., *Transposon Sequencing of Brucella abortus Uncovers Essential Genes for Growth In Vitro and Inside Macrophages.* Infect Immun, 2018. **86**(8).
49. Bandara, A.B., et al., *The putative penicillin-binding proteins 1 and 2 are important for viability, growth and cell morphology of Brucella melitensis.* Vet Microbiol, 2009. **133**(4): p. 387-93.
50. Pazos, M. and W. Vollmer, *Regulation and function of class A Penicillin-binding proteins.* Curr Opin Microbiol, 2021. **60**: p. 80-87.
51. Strobel, W., et al., *Function and localization dynamics of bifunctional penicillin-binding proteins in Caulobacter crescentus.* J Bacteriol, 2014. **196**(8): p. 1627-39.
52. McPherson, D.C. and D.L. Popham, *Peptidoglycan synthesis in the absence of class A penicillin-binding proteins in Bacillus subtilis.* J Bacteriol, 2003. **185**(4): p. 1423-31.
53. Rohs, P.D.A., et al., *A central role for PBP2 in the activation of peptidoglycan polymerization by the bacterial cell elongation machinery.* PLoS Genet, 2018. **14**(10): p. e1007726.
54. Banzhaf, M., et al., *Cooperativity of peptidoglycan synthases active in bacterial cell elongation.* Mol Microbiol, 2012. **85**(1): p. 179-94.
55. Dion, M.F., et al., *Bacillus subtilis cell diameter is determined by the opposing actions of two distinct cell wall synthetic systems.* Nat Microbiol, 2019. **4**(8): p. 1294-1305.
56. Mueller, E.A., et al., *Plasticity of Escherichia coli cell wall metabolism promotes fitness and antibiotic resistance across environmental conditions.* Elife, 2019. **8**.
57. Venturi, V. and C. Keel, *Signaling in the Rhizosphere.* Trends Plant Sci, 2016. **21**(3): p. 187-198.
58. Shi, H., et al., *How to Build a Bacterial Cell: MreB as the Foreman of E. coli Construction.* Cell, 2018. **172**(6): p. 1294-1305.

bioRxiv preprint doi: https://doi.org/10.1101/2021.03.31.437934; this version posted March 31, 2021. The copyright holder for this preprint (which was not certified by peer review) is the author/funder, who has granted bioRxiv a license to display the preprint in perpetuity. It is made available under aCC-BY-ND 4.0 International license.

59. Zupan, J.R., et al., *GROWTH POLE RING protein forms a 200-nm-diameter ring structure essential for polar growth and rod shape in Agrobacterium tumefaciens.* Proc Natl Acad Sci U S A, 2019. **116**(22): p. 10962-10967.
60. Schaper, S., et al., *Seven-transmembrane receptor protein RgsP and cell wall-binding protein RgsM promote unipolar growth in Rhizobiales.* PLoS Genet, 2018. **14**(8): p. e1007594.
61. Kuru, E., et al., *Author Correction: Fluorescent D-amino-acids reveal bi-cellular cell wall modifications important for Bdellovibrio bacteriovorus predation.* Nat Microbiol, 2018. **3**(2): p. 254.
62. Baranowski, C., et al., *Maturing Mycobacterium smegmatis peptidoglycan requires non-canonical crosslinks to maintain shape.* Elife, 2018. **7**.
63. Schoonmaker, M.K., W.R. Bishai, and G. Lamichhane, *Nonclassical transpeptidases of Mycobacterium tuberculosis alter cell size, morphology, the cytosolic matrix, protein localization, virulence, and resistance to beta-lactams.* J Bacteriol, 2014. **196**(7): p. 1394-402.
64. Kieser, K.J., et al., *Phosphorylation of the Peptidoglycan Synthase PonA1 Governs the Rate of Polar Elongation in Mycobacteria.* PLoS Pathog, 2015. **11**(6): p. e1005010.
65. Valbuena, N., et al., *Characterization of HMW-PBPs from the rod-shaped actinomycete Corynebacterium glutamicum: peptidoglycan synthesis in cells lacking actin-like cytoskeletal structures.* Mol Microbiol, 2007. **66**(3): p. 643-57.
66. Joyce, G., et al., *Cell division site placement and asymmetric growth in mycobacteria.* PLoS One, 2012. **7**(9): p. e44582.
67. Lavollay, M., et al., *The peptidoglycan of stationary-phase Mycobacterium tuberculosis predominantly contains cross-links generated by L,D-transpeptidation.* J Bacteriol, 2008. **190**(12): p. 4360-6.
68. Lavollay, M., et al., *The Peptidoglycan of Mycobacterium abscessus Is Predominantly Cross-Linked by L,D-Transpeptidases.* J Bacteriol, 2011. **193**(3): p. 778-782.
69. Morton, E.R. and C. Fuqua, *Laboratory maintenance of Agrobacterium.* Curr Protoc Microbiol, 2012. **Chapter 1**: p. Unit3D 1.
70. Morton, E.R. and C. Fuqua, *Unit 3D.2 Genetic Manipulation of Agrobacterium.* Curr Protoc Microbiol, 2012. **Chapter**: p. Unit-3D.2.
71. Schafer, A., et al., *Small mobilizable multi-purpose cloning vectors derived from the Escherichia coli plasmids pK18 and pK19: selection of defined deletions in the chromosome of Corynebacterium glutamicum.* Gene, 1994. **145**(1): p. 69-73.
72. Howell, M., J.J. Daniel, and P.J.B. Brown, *Live Cell Fluorescence Microscopy to Observe Essential Processes During Microbial Cell Growth.* JoVE, 2017(129): p. e56497.